Physiologia Plantarum

SPPS

ORIGINAL RESEARCH OPEN ACCESS

Pit Membrane Thickness Determines Differences in Embolism Resistance Among *Brassica oleracea* Genotypes

N. Anai Pereira-Zaldívar[1,2] | Giovanni Bortolami[1,3] | Maximilian Larter[4] | Sylvain Delzon[4] | Régis Burlett[4] | Jesse van Haasteren[1] | Manon van Unen[1] | Kevin Wiegant[1] | Salma Balazadeh[5] | Frederic Lens[1,2]

[1]Naturalis Biodiversity Center, Research Group Functional Traits, Leiden, the Netherlands | [2]Plant Sciences, Leiden University, Institute of Biology Leiden (IBL), Leiden, the Netherlands | [3]Plant Ecology Research Laboratory PERL, School of Architecture, Civil and Environmental Engineering ENAC, EPFL, Lausanne, Switzerland | [4]BIOGECO INRAE, Université de Bordeaux, Pessac, France | [5]Molecular Plant Stress Biology, Leiden University, Institute of Biology Leiden, Leiden, the Netherlands

Correspondence: N. Anai Pereira-Zaldívar (n.a.pereira.zaldivar@biology.leidenuniv.nl) | Frederic Lens (frederic.lens@naturalis.nl)

Received: 22 January 2026 | **Revised:** 28 April 2026 | **Accepted:** 18 May 2026

ABSTRACT

As drought events become more severe, understanding drought-tolerance traits in crops is vital for food security. *Brassica oleracea* L., a widely consumed vegetable (including cabbage, cauliflower, and broccoli), has seen a rise in cultivation, but the response of different genotypes to drought remains poorly studied. Here, we investigated the mechanisms underlying drought resistance in seven genotypes of *B. oleracea* (two grandparental lines and five F2 genotypes) by examining stem anatomical and hydraulic traits, as well as stomatal characteristics, leaf dimensions, and stomatal regulation under drought conditions. Detailed measurements of stem anatomical traits were obtained using light and electron microscopy, while stem hydraulic vulnerability was assessed using the Optical Vulnerability method. The seven genotypes displayed contrasting water-use and hydraulic strategies. Under well-watered conditions, initial stomatal conductance ($g_{s\Psi 0}$) showed considerable variation independent of their leaf and stomata size and density, while the leaf water potential at 90% stomatal closure (Ψg_{s90}) was similar among genotypes. Stomatal safety margins (SSM) were positive across genotypes, confirming coordination between stomatal regulation and xylem hydraulics, and mainly driven by stem P_{50}, which was approximately 1 MPa lower in the most tolerant genotype. Embolism resistance was best explained by the thickness of the intervessel pit membrane, highlighting the importance of including anatomical traits in plant drought tolerance studies. To conclude, the intraspecific variation observed in anatomical, hydraulic and stomatal traits among our *B. oleracea* genotypes indicates potential adaptability to drought and suggests that more drought-tolerant genotypes could be identified within this crop species through targeted, human-mediated crosses.

1 | Introduction

One of the main effects of global climate change involves shifts in precipitation patterns towards more unpredictable and extreme drought periods (Yuan et al. 2023). In agriculture, this will play a major role as the impact of longer and more intensive drought periods will pose a serious challenge to safeguard food production in the future (Grigorieva et al. 2023; Ghosh et al. 2024). A better understanding of the mechanisms associated with plants' drought tolerance is therefore essential for developing more drought-tolerant crops that will reduce the negative impact of climate change on crop growth, yield, and survival (Meza et al. 2020; Pereira et al. 2024; Torres-Ruiz et al. 2024). Addressing this challenge requires research into plant–water relations, plant hydraulics, and observations on anatomical traits associated with drought tolerance (Lens et al. 2022; Mantova et al. 2022; McDowell et al. 2022).

A key focus in plants' drought resilience research is the study of hydraulic failure due to gas embolism in water-conducting xylem cells (McDowell et al. 2008; Choat et al. 2012; Lens et al. 2013; Max et al. 2023; Garcia et al. 2023; Alon et al. 2024).

The xylem water potential (xylem pressure), which induces a 50% loss of hydraulic conductivity (P_{50}), has long been used as a proxy for assessing plant vulnerability to drought-induced embolism (Tyree and Sperry 1989; Tyree and Zimmermann 2013). P_{50} is a widely used predictive functional trait in comparative studies, being generally more negative in plants from drier environments (Brodribb and Hill 1999; Maherali et al. 2004; Choat et al. 2012; Lens et al. 2016; Larter et al. 2017). At the intraspecific level as well, substantial variation in P_{50} can be measured across populations thriving in contrasting environments (Kolb and Sperry 1999; Schuldt et al. 2016; López et al. 2016; Volaire et al. 2018; Dória et al. 2019) or across genotypes with contrasting stem anatomical differences (Ahmad et al. 2018; Thonglim et al. 2021, 2023). Whereas the nanoscale mechanisms governing embolism initiation in the xylem sap and its subsequent spread through interconduit pit membranes into the three-dimensional vessel network are not yet fully resolved (Schenk et al. 2015; Zhang et al. 2020, 2024; Kaack et al. 2021; Lens et al. 2022), P_{50} variation in angiosperms has been mainly attributed to variation in the thickness of the intervessel pit membranes rather than vessel diameter (Lens et al. 2011, 2022, 2023; Li et al. 2016; Dória et al. 2018, 2019; Thonglim et al. 2021, Thonglim et al. 2023; Isasa et al. 2023), although there is no single trait that can explain the whole plant drought tolerance. Lethal levels of drought-induced hydraulic failure, from which angiosperms cannot recover, typically occur beyond the P_{50} threshold, at ~88% loss of conductivity (P_{88}), although the physiological thresholds defining the point of no return remain to be precisely determined across a broader range of species and life forms (Urli et al. 2013; Hammond et al. 2019; Mantova et al. 2021, 2022; Brodribb et al. 2021).

Plants can delay catastrophic hydraulic failure by closing their stomata, thereby reducing transpirational water loss and maintaining a more stable xylem water potential (Martin-StPaul et al. 2017; Mantova et al. 2023). However, a decrease in stomatal conductance (g_s) is inherently associated with lower carbon assimilation, which may constrain plant growth and competitiveness (Schönbeck et al. 2022). Therefore, a more integrated way to assess a plant's drought tolerance strategy is to combine stomatal regulation and water-use behavior with xylem hydraulic vulnerability. One way to do this is to calculate the stomatal safety margin (SSM), defined as the difference between the water potential at stomatal closure (Ψg_{s90}) and P_{50} (Skelton et al. 2015; Dayer et al. 2020; Thonglim et al. 2023). Plants with conservative water use strategies, characterized by early and rapid stomatal closure together with embolism-resistant xylem, show a wider and positive SSMs; plants with riskier strategies close their stomata at lower water potential when the xylem has already started to embolize, leading to narrow positive or even negative SSMs (Skelton et al. 2015; Martin-StPaul et al. 2017; Pivovaroff et al. 2018; Thonglim et al. 2023).

Hydraulic studies have mainly focused on woody species, largely overlooking herbaceous species despite their importance in agriculture (Cochard 2002a; Lens et al. 2016; Skelton et al. 2017; Lamarque et al. 2020; Harrison Day and Brodribb 2023; Huang et al. 2024; Pereira et al. 2024). Furthermore, research on herbaceous crop hydraulics that integrates stomatal behavior with detailed anatomical observations is even more limited (Li et al. 2009; Ahmad et al. 2018; Andrade et al. 2022; Harrison Day et al. 2023; Haverroth et al. 2024; Bortolami et al. 2024), which constrains our understanding of the underlying mechanisms behind drought resistance in forbs and grasses (Huang et al. 2024). In the stems of predominantly herbaceous lineages, correlated traits such as intervessel pit membrane thickness, lignification/woodiness levels in stems, and vessel wall thickness are key anatomical traits linked to drought-induced embolism resistance across various lineages (Lens et al. 2011, 2022, 2023; Li et al. 2016; Pereira et al. 2018; Dória et al. 2018, 2019; Thonglim et al. 2021; Thonglim et al. 2023; Zizka et al. 2022; Isasa et al. 2023; Haverroth et al. 2024).

Other drought-associated traits, beyond stomatal closure and stem anatomical characteristics, have been linked to variation in leaf morphology and function. Across environmental gradients, smaller leaves are generally more prevalent in drier ecosystems, reflecting a global pattern of leaf area adaptation to water availability (Yates et al. 2010; Wright et al. 2017). This pattern has often been associated with enhanced resistance to drought-induced embolism, as species with smaller leaves tend to exhibit more negative P_{50} values (Scoffoni et al. 2011; Kröber et al. 2014; Schreiber et al. 2016; Guillemot et al. 2022). Similarly, in perennial woody crop species such as olives and coffee, reduced single-leaf area has been linked to improved hydraulic performance under water deficit (Nardini et al. 2014; Razouk et al. 2022). However, in leafy vegetables such as cabbage, a reduction in leaf size can substantially decrease agricultural yield and, in turn, the amount of marketable biomass. Additional leaf traits, such as stomatal density and size, have been associated with regulation and limitation of transpirational water loss (Drake et al. 2013; Caine et al. 2019, 2023).

In our study, we focused on *Brassica oleracea* L., a globally cultivated species with high nutritional value and pharmacological potential (Stoewsand 1995; Ayaz et al. 2006; Singh et al. 2007), for which selective human-driven breeding has resulted in a wide diversity of cultivars consumed as vegetables (broccoli, cabbage, cauliflower, brussels sprouts, and others) (Rakow 2004). During this century, the agricultural and economic production of cabbage-type *B. oleracea* cultivars has substantially grown (FAO 2023), increasing the need for more research to identify genotypes that are more resistant to drought in the context of plant resilience to climate change (Sahin et al. 2018; Mafakheri and Kordrostami 2020; Ben Ammar et al. 2022).

To assess how stem anatomical and leaf traits jointly contribute to hydraulic safety in *Brassica oleracea* (cabbage), we crossed two parental lines with contrasting stem anatomies and leaf size: a giant woody Jersey Island accession and a small herbaceous TO1000 accession (see Section 2). We then analysed the two lines and five F2 genotypes at an early developmental stage (2-month-old individuals) to determine how variation in xylem anatomy (e.g., T_{PM}: intervessel pit membrane thickness; T_V: vessel wall thickness), stem woodiness (P_{LIG}: proportion of lignified area per total stem area), stem embolism resistance (P_{12}, P_{50}, and P_{88}), drought-induced

and well-watered stomatal behaviour (Ψg_{s90}: stomatal closure threshold and $g_{s\Psi 0}$), and the interaction between drought-induced stomatal behaviour and embolism resistance (SSM: stomatal safety margin) relates to differences in hydraulic safety. In addition, we quantified leaf and stomatal anatomical traits (leaf size, total leaf area, stomatal size, and stomatal density) to assess whether leaf and stomatal dimensions contribute to genotypic differences in stomatal drought response and tolerance to drought-induced embolism. We hypothesised the following: (1) There is genotypic variability in resistance to xylem embolism, which is accounted for or explained by stem anatomical traits, particularly intervessel pit membrane thickness, vessel wall thickness, and the proportion of stem woodiness. (2) Stomatal closure (Ψg_{s90}) is coordinated with stem xylem vulnerability, leading to positive hydraulic safety margins (SSM: $\Psi g_{s90} - P50$). (3) Genotypes with greater stem hydraulic safety (less vulnerable xylem) and/or conservative stomatal behaviour (reduced $g_{s\Psi 0}$ or early Ψg_{s90}) also exhibit water-conservative leaf and stomatal morphological traits (smaller leaves, lower total leaf area, and smaller stomata or lower densities), indicating coordinated regulation between stem and leaves and possible variability in the SSM among genotypes.

2 | Material and Methods

2.1 | Plant Material

We crossed the small, homozygous, small-leaved, fast-flowering, herbaceous *B. oleracea* line TO1000 (Parkin et al. 2014) with the tall, heterozygous, biennial, large-leaved, late-flowering woody walking stick kale (*Brassica oleracea* L. convar. *acephala* (DC.) Alef. var. *viridis* L.) native to Jersey (Channel Islands, UK; hereafter JKC) (Parker and Stevens-Cox 1970). Although the TO1000 line is treated as an herbaceous accession, there is still a clear wood cylinder confined to the base of the stem (for a more elaborate discussion between herbaceous and woody species, see Lens et al. 2012; and Kidner et al. 2016). These two accessions were crossed reciprocally, resulting in F1 seeds from both parents (see Vos et al. 2022 for more information). Afterward, an early-flowering F1 was crossed with a late-flowering F1, leading to about 200 F2 genotypes. All genotypes were grown from in vitro tissue culture. We selected five F2 genotypes (18174, 18168, 18187, 18326, and 18367) and the two grandparents along a tolerant-to-sensitive gradient based on a pilot drought experiment where we fast-screened stomatal conductance and water potential decline across all 200 F2 genotypes and the two grandparents (Figure S1, van Haasteren et al. 2019). A second criterion for selecting the F2s focused on only including genotypes that kept the leaves attached to the main stem for longer periods under drought stress conditions, thereby avoiding early disconnection between the petioles and the main stem.

2.2 | Growth Conditions

The seven *B. oleracea* genotypes are available as tissue culture plants in a dedicated growth chamber at the Institute of Biology Leiden (Leiden University, The Netherlands). The tissue-culture plants are stored in sterile test tubes with 4 mL nutrient-rich agar medium. Every 2 to 3 months, the plantlets were multiplied in vitro by cutting parts of the internodes between leaves from the previous tissue culture batch. The cloned plant parts were then placed again in sterile test tubes with agar medium until the internodes had grown into plantlets with a developing root system and visible stem elongation. After 2 months in the tubes, the plantlets with sufficient root system development were transferred from the agar medium to soil (100% basis biomix composed of 65% peat and 35% organic matter, pH 5.2, Lensli Substrates). We selected a 3 L pot size to ensure the root system would not fully occupy the pot at the 2-month-old stage. The potted plants grew for two months in well-watered conditions inside a controlled growth chamber at 20°C and 70% relative humidity, with a daily 16/8-h light/night cycle at 200 μmol m^{-2} s^{-1} photosynthetically active radiation and watered every second day until the beginning of the experiments. Two months after potting, the experiments started.

2.3 | Xylem Vulnerability to Embolism in Stems

2.3.1 | Optical Vulnerability Method

For each plant, the soil was gently washed from the roots to speed up the dehydration process during the experiment. After cleaning, the roots were temporarily wrapped in wet tissue to prevent rapid dehydration before the data recording started. A section of 30 mm length of bark (< 1 mm thick) was carefully removed from the stem to expose the xylem. To improve light transmission and protect the exposed xylem from dehydration, we immediately covered the exposed xylem with a hydrogel layer (Tensive Gel; Parker Laboratories Inc.). We then placed the stem and hydrogel on a flatbed scanner (V850 Perfection Pro Scanner, Epson Corp.) and used duct sealer clay (Oil-Based Compound, DS1, Panduit) over the scanner's glass to hold the setup in place (Figure S2). The embolism events in the exposed stem xylem were then recorded with the flatbed scanner in a 30 × 10 mm region of interest, using the OpenOV_AutoScan IT script (PhenoBois 2026) to capture an image every 5 min until the exposed xylem area was fully embolised. Simultaneously, the stem xylem water potential was recorded every 30 min for each plant using a stem psychrometer (PSY1, ICT International) placed at the base of the stem. Water potential was measured once a day during the first days of the experiment using a pressure chamber (Model 1515D, PMS Instruments) to verify the accuracy of the stem psychrometer. As the TO1000's stem was too thin for the stem psychrometer and the leaves were challenging (small and fragile) for the pressure chamber, we mainly used the PSYPRO water potential system (Wescor Inc.) to monitor water potential. The results of this device were also verified with the pressure chamber during the first 2 days of drought. The entire OV method took 1 week for most genotypes, while TO1000 was fully embolized at day 3. After all embolism recordings were finalized, we conducted the image analysis in ImageJ (Fiji) (Schindelin et al. 2012) (see http://www.opensourceov.org/). When the xylem sap inside a particular vein transitions to vapor, this is captured by differences in the light transmission (recorded as pixel differences) in the subsequent images. The accumulation of these pixel differences

was then transformed into a percentage of embolised pixels as a proxy of the percentage loss of conductivity due to embolism, estimated with other methods based on water transport measurements. The subsequent images were linked with the associated water potential values through time to build the vulnerability curves of each plant (3–4 plants per genotype) (Brodribb et al. 2016, 2017).

2.3.2 | Cavitron Centrifuge Method

We analysed the stems of four out of the seven genotypes with the Cavitron centrifuge to verify the accuracy of the results obtained with the OV method. The Cavitron is a custom-built centrifuge that allows measuring the water flow through the stems while applying negative pressure to the central part of the stem via increasing centrifugal force (Cochard 2002b; Cochard et al. 2005). The selection criteria were based on the length of the main stem. At the 2-month-old developmental stage, only TO1000 ($n=7$), JKC ($n=1$), 181326 ($n=3$), and 18187 ($n=4$) had the stem length required to fit the Cavitron centrifuge's rotor. For TO1000, seven stems were combined to achieve sufficient hydraulic conductivity during the centrifugation experiment, yielding a single vulnerability curve for this genotype. Also, only one replicate for the JKC grandparent was analysed due to problems with plant growth when transferring the plants from tissue culture to soil.

Before the Cavitron measurements, the complete stem of each plant was harvested at the Institute of Biology Leiden. The leaves were removed while the whole stem was submerged in a water container. Subsequently, the stems were immediately wrapped in wet tissue paper with the roots still attached, bagged in black plastic bags to avoid dehydration, and shipped to the PHENOBOIS platform (INRAE, University of Bordeaux, France) for measurements with the standard cavitron rotors (27 and 39 cm). A reference ionic solution of 10 mM KCl and 1 mM $CaCl_2$ in deionized ultrapure water was used to estimate the maximum hydraulic conductance of the stem in its native state (K_{max} in $m^2\,MPa^{-1}\,s^{-1}$) under xylem pressure close to 0 MPa. The rotation speed was then increased to reach a lower xylem water potential in steps of −0.2 or −0.4 MPa. The hydraulic conductivities at each xylem pressure step (K) were measured using Cavisoft software (Cavisoft v1.5), with the percentage loss of conductivity (PLC) at each pressure step determined as:

$$PLC = 100 \times \left(1 \left(K / K_{max}\right)\right)$$

2.3.3 | Reconstructing Embolism Vulnerability Curves

For both the OV and the Cavitron methods, vulnerability curves were fitted to show the (measured or simulated) change in the percentage loss of conductivity against the stem water potential to estimate the P_{50} value as a proxy of stem vulnerability to embolism. Sigmoid functions (Pammenter and Vander Willigen 1998) were fitted to the data of each plant sample per genotype using the NLIN procedure in SAS 9.4 (SAS 9.4; SAS Institute) following the equation:

$$PLC = 100 / \left[1 + \exp\left((S/25) \times \left(P - P_{50}\right)\right)\right]$$

where S is the slope of the vulnerability curve at the inflexion point (P_{50}), and P is the xylem pressure applied at each step. The parameters S and P_{50} were averaged for each genotype.

2.4 | Stomatal Regulation and Hydraulic Coordination Traits

2.4.1 | Water Potential and Stomatal Conductance (g_s)

Three (F2 genotype 18174 and grandparent JKC) or five plants (for the other five genotypes studied) per genotype were submitted to a drought treatment of at least 12 days without watering. A control batch with the same number of plants per genotype was kept under well-watered conditions. The plants remained in pots under the same environmental conditions in the climate chamber as those in which they were grown at the Institute of Biology Leiden. Both drought treatment and control plants were randomly distributed on climate chamber tables under the same controlled environmental conditions. We measured the plant's water potential with the pressure chamber in previously bagged leaves every second day in a fully expanded mature leaf, meaning our measurements reflected the stem's water potential as the transpiration stream in the measured leaf stopped. For TO1000, the pressure chamber was used only on the first day of the experiment to validate the PSYPRO device, which was used throughout the experiment due to difficulties in safely measuring this genotype with the pressure chamber (because of the small, fragile leaves). At the same time, g_s ($mmol\,H_2O\,m^{-2}\,s^{-1}$) was recorded daily with an LI-600 porometer/fluorometer (Li-Cor) in Auto Mode configuration. The g_s measurements were repeated daily up to three times in a single mature leaf (5–6th leaf from the stem apex), in the middle section of the leaf, and between the margin and the midrib. Before the onset of drought (i.e., water potential ≤ -1 MPa), we did not find significant differences in g_s between control and drought-treated plants per genotype (Figure S3A). A sigmoid function was fitted to build one g_s curve per genotype, while the water potential dropped during drought, using the following equation with the NLIN procedure in SAS:

$$g_s = g_{s\Psi 0} / \left[1 + \exp\left(S \times \left(\Psi - \Psi g_{s50}\right)\right)\right]$$

where $g_{s\Psi 0}$ is the maximal stomatal conductance at water potential approaching zero, S is the slope, and Ψg_{s50} is the water potential at 50% of stomatal closure. The g_s curves per genotype were then transformed into percentages to estimate the water potential value at 90% of stomatal closure (Ψg_{s90}). The Ψg_{s90} was used to estimate the drought intensity leading to stomatal closure.

2.4.2 | Stomatal Safety Margin

Following Martin-StPaul et al. (2017), and Thonglim et al. (2023), the stomatal safety margin (SSM) for each genotype was estimated as the difference between Ψg_{s90} and the P_{50} values from the OV-based stem vulnerability curves, according to the following equation:

$$SSM = \Psi g_{s90} - P_{50}$$

2.5 | Stem Anatomy

2.5.1 | Light Microscopy

Three to five stems per genotype were cut into 3–5 cm length segments from the well-water control plants at the end of the drought experiment. The samples were taken close to the base of the stem at a similar height to the section scanned during the OV method to match the P_{50} measurements from the OV technique. The stem samples were fixed in 70% ethanol and cut into transverse sections of 20–30 μm using a sliding microtome (Reichert). Following Lens et al. (2005), the sections were then bleached with sodium hypochlorite 1%–3%, rinsed with water, stained with safranin (0.5% in 50% ethanol) mixed with alcian blue (1% in water) (35%–65%), and dehydrated in an ethanol series (50%, 70%, and 96%). We used Histo-clear as a clearing agent before the sections were mounted in Euparal green. A Zeiss Axio Imager D2 (Axio Imager M2, Zeiss) was used to photograph xylem traits at 40× magnification (Table 1). A Zeiss modular stereo microscope (ZEISS SteREO Discovery. V20, Zeiss) was used to photograph the proportion of stem tissues in a cross-section at 28 to 115× magnifications (Table 1). The pictures were analysed with ImageJ.

2.5.2 | Transmission Electron Microscopy

We harvested a sample of 1 cm in length from the bottom of the bigger stem samples taken for light microscopy before they were deposited in ethanol for three stems per genotype and immediately submerged them in Karnovsky's fixative (Karnovsky 1965) after slicing the sample multiple times longitudinally. The 1 cm sliced samples were transferred to 0.1 M cacodylate buffer, post-fixed with 1% buffered osmium tetroxide and rinsed with buffer solution. We used 1% uranyl acetate for staining and subsequently dehydrated the samples in a series of ethanol: 1% uranyl acetate replacement (30%, 50%, 70%, 96% ethanol and twice in 100% ethanol). The stained samples were infiltrated with Epon 812 (Electron Microscopy Sciences, Hatfield, UK) and placed in the oven at 60°C for 48 h. We used a rotary microtome with a glass knife to trim the Epon blocks into 2 μm-thick sections. Subsequently, we used a Leica EM UC7 ultramicrotome with a diamond knife to cut the sections with vessel–vessel contact areas into ultrathin sections of 90–95 nm in thickness. The sections were dried and mounted on film-coated copper slot grids with Formvar coating (Agar Scientific), and then post-stained with uranyl acetate and lead citrate. Ultrastructural observations of intervessel pits were performed and photographed using a JEM-1400 Plus transmission electron microscope (TEM) (JEOL) equipped with an 11-megapixel camera (Quemesa, Olympus). We measured the intervessel pit membrane thickness (min. 32 pits per genotype) and pit chamber depth (min. 13 pits) with ImageJ in non-shrunken intervessel pit membranes from two to three individuals per genotype (Table 1).

2.6 | Leaf Traits

2.6.1 | Leaf Size, Leaf Number, and Total Leaf Area

The average leaf size for each genotype was calculated based on the individual area of multiple mature leaves ($n = 3$–5 per genotype) from the well-watered control batch. The area was measured by outlining a mature, well-watered leaf on a paper sheet. The leaf outline with scale reference was scanned in a flatbed scanner, and its area was calculated using the polygon selection tool in ImageJ. We estimated the leaf number per genotype by counting all fully unfolded leaves per individual ($n = 3$–5 per genotype) from each genotype from the well-watered control batch. To estimate the total leaf area per plant, we multiplied the leaf size and leaf number (Table 1). Stem anatomical traits and leaf traits were measured in 2-month-old well-watered controls to avoid any effect of drought-induced tissue damage. This means that these plants were different from the 2-month-old plants that were used in the stem hydraulics and stomatal regulation during drought measurements.

2.6.2 | Stomata Anatomy

The stomatal density, length, and width were measured from (both adaxial and abaxial) epidermal imprints from a mature leaf in three individuals per genotype. To create the imprints, we applied transparent nail varnish to a leaf surface area of 3 × 3 cm in a similar position as the area used to measure g_s (Hilu and Randall 1984). After 3–5 min, the dried varnish was removed by pressing and lifting a piece of transparent adhesive tape. The imprints were then placed on a microscope slide. Three to five non-overlapping fields of view were photographed with the Axio Imager D2 at 40× magnification and measured with ImageJ. Stomatal density (per mm^2) was calculated based on the number of stomata counted in the area of the field of view (Table 1).

2.7 | Statistical Analysis

First, we tested for statistically significant differences in stem embolism resistance (P_{50}), stem hydraulic traits (P_{12} and P_{88}), leaf and stem anatomical features (Table 1), and stomatal regulation and hydraulic coordination traits ($g_{s\Psi 0}$, Ψg_{s90} and SSM) among the genotypes studied, by running linear mixed models in the *nlme* package (version 3.1, R Studio version 2024.04.2) (Pinheiro 2011). We set the genotype and the studied traits as fixed effects, and the individual plants as random effects, since multiple measures were taken on each plant. For each model, we used the *emmeans* package (version 4.0.3) (Lenth et al. 2018) to perform pairwise comparisons with estimated marginal means (Searle et al. 1980) with Benjamini and Hochberg adjustment (Benjamini and Hochberg 1995). Pearson's index was applied with the *psyche* package (2.4.6.26) to study the correlation among the traits mentioned above. Then, linear multiple regression models were built using the stem anatomical traits (predictive variables) with a significant correlation to stem hydraulic traits (P_{50}, P_{12}, and P_{88}), and leaf anatomical traits with stomatal regulation and hydraulic coordination traits ($g_{s\Psi 0}$, Ψg_{s90}, and SSM). We selected our predictors using previous knowledge and a collinearity analysis with the variance inflation factor (VIF). Subsequently, a two-way stepwise model selection was followed with the *Stats* package (4.5.0) to remove the least predictive variables according to the Akaike information criterion (AIC). We calculated the relative importance of each independent variable in the models using the Lindeman, Merenda and Gold (1980) method in the *relaimpo* package (2.2-7). After obtaining our final regression models, we used mixed-effects models and Pearson's

TABLE 1 | List of measured stem anatomical traits and leaf traits with their acronym, definition and measurement details.

Acronym	Definition	Calculation	Number of measurements	Unit	Technique
A_F	Fibre cell area	Area of a single xylem fibre in cross-section	Min. 30 fibres	μm^2	LM
A_{FL}	Fibre lumen area	Area of single xylem fibre lumen in cross-section	Min. 30 fibres	μm^2	LM
A_{FW}	Fibre wall area	A_F-A_{FL} for the same fibre	Min. 30 fibres	μm^2	LM
A_{LIG}	Lignified stem area	Total xylem area + fibre caps area in cross-section	Min. 3 stems per accession	mm^2	LM
A_{PITH}	Pith area	Total pith area in cross-section	Min. 3 stems per accession	mm^2	LM
P:X	Pith to xylem ratio	Proportion of pith area per xylem area	Min. 3 stems per accession		LM
A_S	Total stem area	Total stem area in cross-section	Min. 3 stems per accession	mm^2	LM
D	Vessel diameter	$D=(4A)/\pi$, where A is the vessel lumen area	50 vessels	μm	LM
D_{MAX}	Maximum vessel diameter	Diameter of the lumen of a single vessel in cross-section	Min. 16 vessels	μm	LM
D_{PC}	Pit chamber depth	Distance from the relaxed pit membrane to the pit chamber roof near the inner pit aperture	Min. 13 pits	μm	TEM
$P_{FW}F_A$	Proportion of fibre wall area per fibre cell area	A_{FW}/A_F for the same fibre: a measure of xylem fibre wall thickness	Min. 30 fibres		LM
P_{LIG}	Proportion of lignified area per total stem area	A_{LIG}/A_s	Min. 3 stems per genotype		LM
T_{PM}	Intervessel pit membrane thickness	Thickness of the intervessel pit membrane	Min. 32 pits	μm	TEM
T_V	Vessel wall thickness	Thickness of a single vessel wall	Min. 16 vessels	μm	LM
T_{VW}/D_{MAX}	Thickness to span ratio of vessels	Double intervessel wall thickness divided by the maximum diameter of the largest vessel measured in perpendicular direction	Min. 16 vessels	μm	LM
D_V	Vessel density	Number of vessels per mm^2	Min. 7 measurements	No. of vessels/mm^2	LM
D_{SAB}	Abaxial stomatal density	Number of stomata in the abaxial epidermal surface per mm^2	Min. 6 mm^2measurements	No. of stomata/mm^2	LM
L_{SAB}	Abaxial stomatal length	Total length of a single stoma in the abaxial epidermal surface	Min. 180 stomata	μm	LM
W_{SAB}	Abaxial stomatal width	Total width of a single stoma in the abaxial epidermal surface	Min. 180 stomata	μm	LM

(Continues)

TABLE 1 | (Continued)

Acronym	Definition	Calculation	Number of measurements	Unit	Technique
D_{SAD}	Adaxial stomatal density	Number of stomata in the adaxial epidermal surface per mm^2	Min. 6 measurements	No. of stomata/mm^2	LM
L_{SAD}	Adaxial stomatal length	Total length of a single stoma in the adaxial epidermal surface	Min. 180 stomata	μm	LM
W_{SAD}	Adaxial stomatal width	Total width of a single stoma in the adaxial epidermal surface	Min. 180 stomata	μm	LM
S_{Leaf}	Leaf size	Size measured as the area of a leaf	Min. 3 leaves	cm^2	—
N_{Leaf}	Number of leaves	Number unfolded and fully developed of leaves per plant	Min. 3 plants	No. of leaves	—
T_{Leaf}	Total leaf area per plant	$S_{Leaf} \times N_{Leaf}$	Min. 3 plants	cm^2	—
P_{50}	Xylem water potential inducing 50% loss of hydraulic conductivity or embolised pixels	Pressure inside the xylem at which 50% of the pixels are embolised (see Section 2)	3–4 plants	MPa	VC
P_{88}	Xylem water potential inducing 88% loss of hydraulic conductivity or embolised pixels	Pressure inside the xylem at which 88% of the pixels are embolised (see Section 2)	3–4 plants	MPa	VC
P_{12}	Xylem water potential inducing 12% loss of hydraulic conductivity or embolised pixels	Pressure inside the xylem at which 12% of the pixels are embolised (see Section 2)	3–4 plants	MPa	VC
$Slope_{VC}$	Slope of the vulnerability curve	Slope of the average optical vulnerability curve	3–4 plants	MPa	VC
Ψg_{s90}	Xylem water potential inducing 90% reduction of stomatal conductance	Pressure inside the xylem at which 90% of stomatal conductance is lost (see Section 2)	3–4 plants	MPa	SCC
g_s	Stomatal conductance	Direct measurement with Li-600 porometer	3–5 plants	mmol H_2O m^{-2} s^{-1}	PM
$g_{s\Psi 0}$	Maximum stomatal conductance at the highest water potential	Maximum g_s value measured with the Li-600 porometer at the highest water potential value in the g_s decline during drought curve	3–5 plants	mmol H_2O m^{-2} s^{-1}	PM
SSM	Stomatal safety margin	$\Psi g_{s90} - P_{50}$	3–4 plants	MPa	VC and SCC

Note: Min. three stems per genotype ($n = 3–5$).
Abbreviations: LM, light microscopy; PC, pressure chamber; PM, porometer; PSY, psychrometer; SCC, stomatal conductance curve; TEM, transmission electron microscopy; VC, vulnerability curve.

coefficient to estimate the correlation of the random effects of the dependent and independent variables. This step strengthened our analysis since variables were averaged by genotype from different datasets: a hydraulic and a stomatal regulation dataset from drought treatment experiments, along with an anatomical dataset from well-watered plants. Results were considered significant when $p < 0.05$.

3 | Results

3.1 | Stem Vulnerability to Embolism

The stem P_{50} among the seven genotypes measured with the optical vulnerability (OV) technique varied from −2.11 to −3.06 MPa (Figure 1; Table 2). These results were supported by similar stem P_{50} values obtained with the Cavitron centrifuge

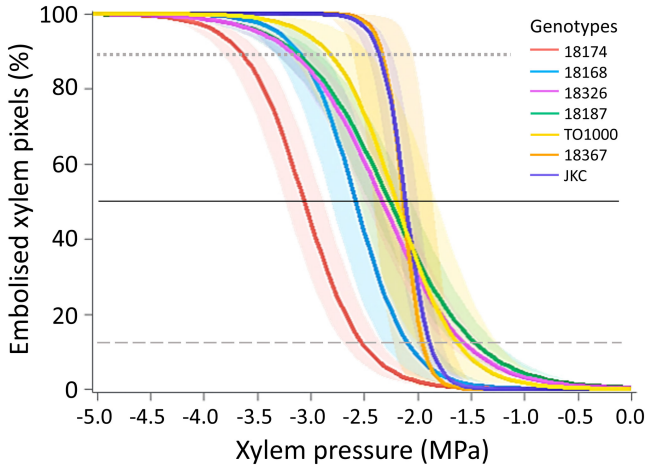

FIGURE 1 | Mean stem optical vulnerability (OV) curves for each *B. oleracea* genotype constructed by plotting the percentage of embolised xylem pixels as a function of xylem pressure (MPa). Thick-colored curves correspond to average values and shaded bands to the standard error in the genotype-specific vulnerability curves (based on three to four individuals). The black solid line shows the pressure that induces 50% of embolised pixels in the xylem vessels (P_{50}), and the grey dashed and dotted lines show P_{12} and P_{88}, respectively.

for genotypes 18187, 18326, JKC, and TO1000 (Figure S4). Based on the OV measurements, significant differences in stem P_{50} were detected among genotypes, with the F2 genotype 18174 showing significantly higher embolism resistance ($P_{50} = -3.06 \pm 0.18$ MPa) than all other genotypes (18187, 18326, 18367, JKC, TO1000, $p < 0.05$, Figure S3B). In contrast, the most embolism-vulnerable genotype was the JKC grandparent, with P_{50} values very close to the other four remaining sensitive genotypes ($P_{50} = -2.11 \pm 0.11$ MPa) (Figure 1; Table S1 and Figure S3B). Additionally, we found strong positive correlations between P_{50} and P_{12} and P_{88} ($R = 0.76$ and $R = 0.86$, respectively; Figure S5).

3.2 | Stomatal Regulation and Hydraulic Coordination

Under well-watered conditions, genotype 18174 showed the lowest stomatal conductance (387 mmol H_2O m^{-2} s^{-1}; Figure 2, Table 2). Genotypes 18367, 18326, and TO1000 displayed intermediate values (718, 793, and 805 mmol H_2O m^{-2} s^{-1}, respectively; Figure 2, Table 2), while 18168, JKC, and 18187 presented the highest stomatal conductance, ranging from 946 to 1397 mmol H_2O m^{-2} s^{-1} (Figure 2; Table 2; Figure S3A). For Ψg_{s90}, the values were rather similar across the seven genotypes studied. TO1000 had higher Ψg_{s90} than 18187 and 18326 ($t = -4.1$, $p < 0.05$ and $t = -2.6$, $p < 0.01$, respectively; Figure S3C) (Table 2; Figure 2), meaning it closed the stomata earlier than these two genotypes. Regarding the stomatal safety margin (SSM), all genotypes showed positive values, ranging from 0.85 to 1.82 MPa, which were primarily driven by the difference in stem P_{50} across the genotypes (Table 2; Figure 2). Consistent with this, genotype 18174 had the widest SSM (1.82 MPa), corresponding to its highly embolism-resistant stem (lower stem P_{50}) (Figure 2; Figure S3B,C).

3.3 | Anatomical Variation and Correlations in Stem, Secondary Xylem, and Leaf Traits Among Genotypes

Vessel wall thickness (T_V) was significantly different among genotype 18174 and the two grandparental lines, while the remaining F2 lines showed similar values ($F = 15.46$; $p = 1.89e^{-05}$;

TABLE 2 | Stem and leaf hydraulic traits of the *B. oleracea* genotypes.

Genotype	P_{88} (MPa)	P_{50} (MPa)	P_{12} (MPa)	$Slope_{VC}$	Ψg_{s90} (MPa)	SSM (MPa)	$g_{s\Psi0}$ (mmol H_2O m^{-2} s^{-1})
18174	−3.61	−3.06	−2.51	90.9	−1.24	1.82	386
18168	−3.07	−2.58	−2.08	101.2	−1.30	1.27	946
18326	−3.11	−2.33	−1.55	64.1	−1.43	0.90	793
18187	−3.07	−2.26	−1.45	61.5	−1.30	0.96	1397
TO1000	−2.79	−2.20	−1.62	85.5	−1.03	1.17	805
18367	−2.32	−2.14	−1.95	273.8	−1.29	0.85	717
JKC	−2.35	−2.11	−1.88	216.7	−1.23	0.89	1144

Note: P_{88}, P_{50} and P_{12} refer to the water potential at 88%, 50% and 12% loss of hydraulic conductivity in stems, respectively, from the optical vulnerability curve in Figure 1. Min. three individuals per genotype ($n = 3$).
Abbreviations: $g_{s\Psi0}$, stomatal conductance from the maximum value of water potential (maximum g_s value) in Figure 2A; $Slope_{VC}$, slope of the optical vulnerability curve; SSM, stomatal safety margin; Ψg_{s90}, water potential at 90% of stomatal closure.

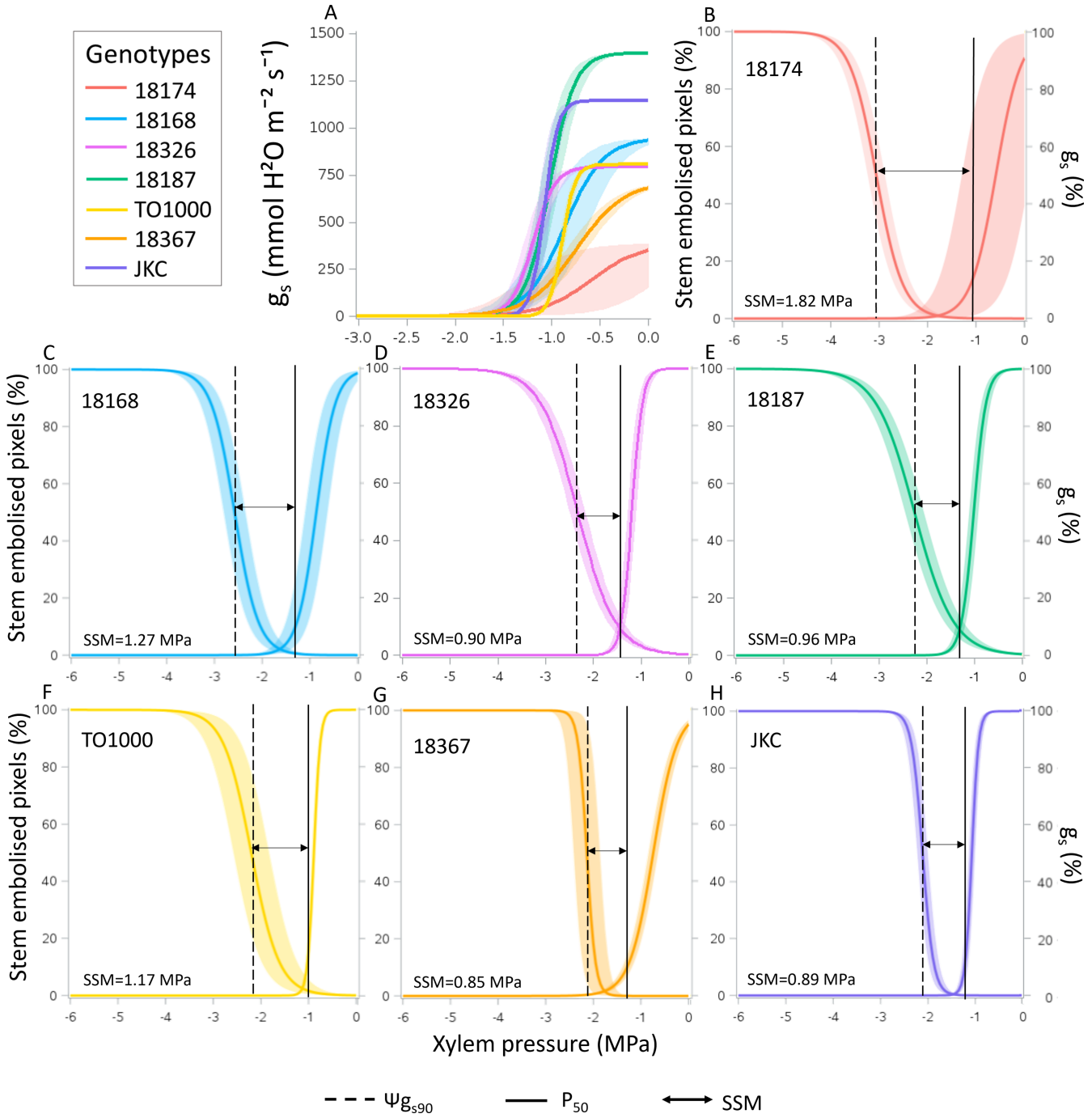

FIGURE 2 | Stomatal regulation and hydraulic coordination of the *B. oleracea* genotypes. (A) Stomatal conductance (g_s) reduction as a response to xylem pressure decline during drought among the seven genotypes (the maximum g_s value at the highest water potential value in the curve was considered the average $g_{s\Psi 0}$ per genotype). (B–H) Graphs showing the percentage of embolised pixels in the stem xylem (curve on the left) and the percentage of g_s (curve on the right) as functions of stem xylem pressure used to estimate each genotype's stomatal safety margins (SSM). The dashed lines represent xylem pressure (water potential in bagged leaves) at 90% loss of stomatal conductance (Ψg_{s90}). The solid lines show the xylem pressure at which 50% of hydraulic conductivity is lost (P_{50}). The difference between the dashed and the solid line refers to the SSM. See Table 2 for the mean values of each trait per genotype, and Table S1 for the standard errors.

Figure S6C). The vessel density (D_V) was higher in genotype 1867 and lower in 18168, when compared to the F2s ($F = 14.29$; $p = 2.97e^{-05}$; Figure S6D). The ratio of vessel wall thickness to vessel diameter (T_{VW}/D_{MAX}) followed a pattern similar to that of T_V, however, for this trait, the TO1000 grandparent showed the lowest value ($F = 8.938$; $p = 0.0004$; Figure S6E). The intervessel pit membrane thickness (TPM) was higher in genotypes 18174 and 18168 compared to the other genotypes (Figure 3V-AB; $F = 38.05$; $p < 2e^{-16}$; Figure S6N). In addition, all genotypes exhibited vestured pits, as shown in Figure 3V-AB. We did not find significant differences in other detailed xylem anatomical traits; for instance, in the proportion of fiber wall area per fiber cell area ($P_{FW}F_A$), fiber wall area (A_{FW}), or vessel diameter (D, D_{MAX}) (Figure S6). Interestingly

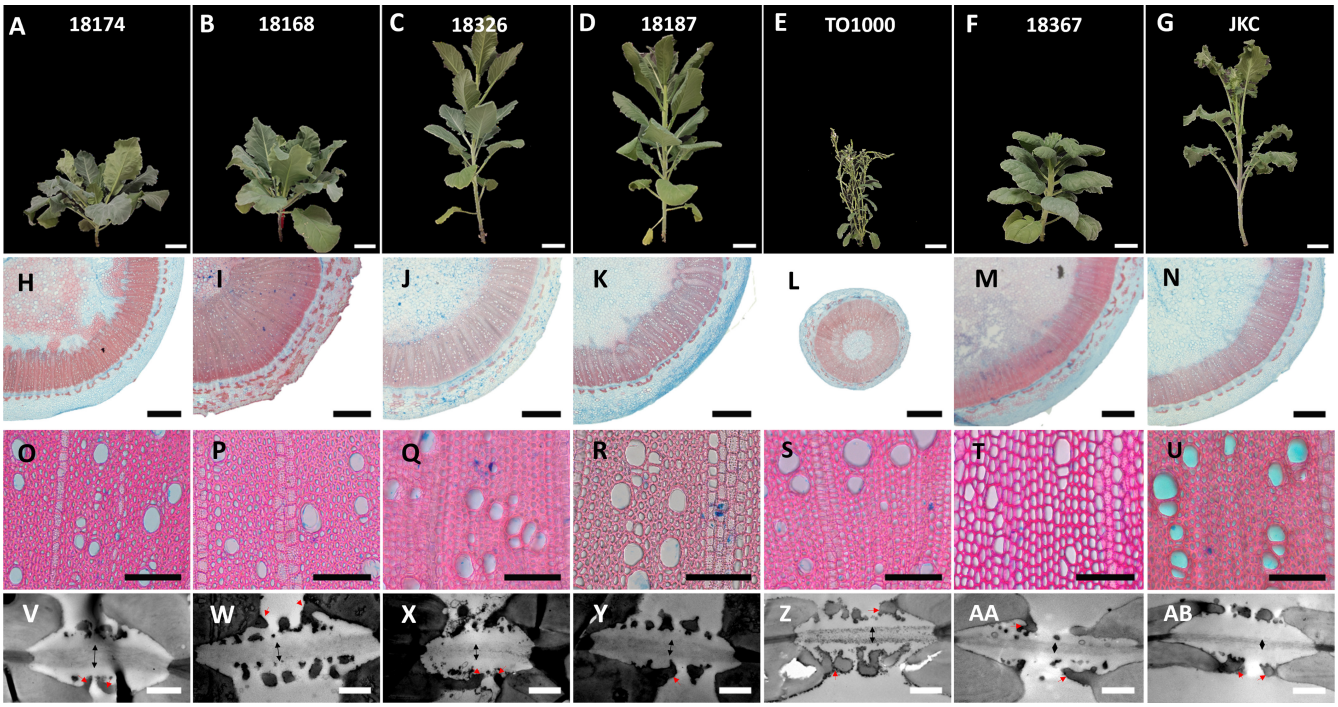

FIGURE 3 | Growth form showing the two grandparental lines (A, B) and five *B. oleracea* F2 genotypes (C–G), along with light microscope cross-sections of their stems (H–N) and wood cylinder (O–U), and transmission electron microscope sections of intervessel pits (V-BB). Black double arrows in V-AB show the thickness of the pit membrane (T_{PM}), and red arrows point to the presence of vestures projecting from the border of the pit aperture. Scale bars equal 10 cm (life forms, A–G), 1000 μm (stem sections, H–N), 100 μm (wood sections, O–U), or 1 μm (pit sections, V-AB).

(T_{VW}/D_{MAX}) was positively correlated with T_V, but not with D_{MAX} (Figure S5).

The stem area (A_S) was similar for 18367, JKC and 18174, and for 18187, 18168 and 18326 ($F = 28.3$; $p = 2.09e^{-15}$; Figure S6G). A similar pattern was found in pith area (A_{PITH}) ($F = 5.58$; $p = 0.0001$; Figure S6I) and pith to xylem ratio (P:X) ($F = 3.714$; $p = 0.004$; Figure S6J). Lignified area per total stem area (P_{LIG}) was similar for 18168, TO1000 and 18326 with higher values, while 18174, JKC and 18367 shared similar lower values (Figure 3H–N; $F = 3.082$; $p = 0.01$; Figure S6L). The lignified stem area (A_{LIG}) was similar among all genotypes except for TO1000, with the lowest value ($F = 4.2$; $p = 0.001$; Figure S6M). Regarding stem and xylem trait correlations, P_{LIG} showed no significant associations with other xylem traits except for a negative correlation with V_D. Similarly, A_{LIG} was positively correlated with T_V but not with any other xylem traits. Among the stem traits, A_S was negatively correlated with P_{LIG} and positively correlated with both A_{PITH} and P:X. Apart from its negative association with A_{PITH}, P_{LIG} showed no additional correlations with stem traits (Figure S5).

Genotypes differed significantly in all leaf traits (Figure S7A–C). Leaf size (S_{Leaf}) was largest in 18174, JKC and 18168 (172–144 cm^2), and smallest in TO1000 (7 cm^2). Leaf number (N_{Leaf}) was highest in TO1000 (96) and lowest in JKC (8). Total leaf area (T_{Leaf}) followed a similar pattern to S_{Leaf}, with genotypes bearing larger leaves (18168 and 18174) showing higher T_{Leaf} (2360 and 2351 cm^2), except for JKC, which, despite its high leaf area, had the second lowest T_{Leaf} (1288 cm^2) due to its reduced number of leaves (see Table S1 for all average values and standard error). In general, genotypes with bigger leaves tended to have fewer leaves and vice versa, as S_{Leaf} and N_{Leaf} showed a negative correlation (Figure S5).

Additionally, genotypic variation in stomatal anatomical traits was observed on both leaf surfaces (Figure S7D–I). On the abaxial surface, stomatal density (D_{SAB}) did not differ significantly among genotypes; however, according to the observed pattern, the density was highest 18174 (335 mm^2) and lowest in 18367 (208 mm^2), while stomatal width (W_{SAB}) and length (L_{SAB}) showed a significant decreasing trend from JKC (12 μm) to 18174 (8 μm) and TO1000 (21 μm) to 18174 (15 μm), respectively. On the adaxial surface, stomatal density (D_{SAD}) differs significantly among genotypes, from the highest 18174 (295 mm^2) to the lowest 18168 (146 mm^2), whereas width (W_{SAD}) and length (L_{SAD}) both vary significantly, showing similar patterns to the abaxial surface (Figure S7E–I). Abaxial and adaxial stomatal densities, lengths and widths were positively correlated. The negative correlation between the abaxial stomatal density (D_{SAB}) and stomatal length (L_{SAB}) indicates that the genotypes have either higher amounts of small stomata on their leaves or fewer larger ones. Likewise, the negative correlation between leaf size (S_{Leaf}) and L_{SAB} seems to indicate that genotypes with big leaves have smaller stomata (Figure S5).

3.4 | Xylem and Stem Anatomical Traits Accounting for the Variation in Vulnerability to Embolism

According to Pearson's coefficient, stem P_{50} showed a strong and significant negative correlation with T_{PM} and T_{VW}/D_{MAX} ($R = -0.93$, $p < 0.01$ and $R = -0.82$, $p < 0.05$, respectively; Figure S5). Linear

regression models supported these results and confirmed that both variables accounted for the variation in P_{50} (T_{PM} $R^2 = 0.87$, $p < 0.05$ and T_{VW}/D_{MAX} $R^2 = 0.67$, $p < 0.05$; Figures 4A,B and S8A,B). Both anatomical variables were retained by the most parsimonious significant multivariate model with stepwise selection accounting for the variation in P_{50} among the genotypes (AIC = −6.4, Table S2). T_{PM} had a higher relative importance for P_{50} (56.3%) than T_{VW}/D_{MAX} (36%) (Figure 4C). No other stem anatomical traits correlated with T_{PM}, while only T_V correlated with T_{VW}/D_{MAX} (Figure S5). We did not find correlations between P_{50} and P_{LIG} or with other stem anatomical traits studied (Figure S5). For example, the lack of correlation between P_{50} and P_{LIG} was evident as the genotype with the most negative P_{50} (18174) did not show high stem lignification (P_{LIG}) (Figures 3H and S6L), but had thicker T_{PM} and vessel walls (T_V) with consequently higher T_{VW}/D_{MAX} values than the other genotypes (Figure S6C,E,N). However, a pilot experiment using the Cavitron centrifuge with a limited sample size ($n = 1$) for the 8-month-old JKC genotype revealed a considerably lower P_{50} (−3.8 MPa) compared to the younger 2-month-old plants (−2.3 MPa). This shift occurred alongside an 8% increase in P_{LIG} in the older JKC individuals (Figure 5). Stem P_{12} only showed a significant correlation to T_{VW}/D_{MAX} ($R = -0.87$, $p < 0.05$, Figure S5) and was retained together with A_{FW} and T_{PM} (relative importance to P_{12} of 48.8%, 29.2%, and 19.5%, respectively, Figure S8C) by the most parsimonious significant P_{12} model ($R^2 = 0.98$, AIC = −11.1, Table S3). Stem P_{88} was positively correlated to T_{PM} ($R = -0.88$, $p < 0.01$) and was the only variable retained by the most parsimonious significant P_{88} model ($R^2 = 0.77$, AIC = 3.7, Table S4). No significant correlation was found between embolism resistance, stomatal conductance or SSM and S_{Leaf}, N_{Leaf} or T_{Leaf} (Figure S5). However, both N_{Leaf} and T_{Leaf} showed significant negative and positive correlations, respectively, with Ψg_{s90} (Figure S5). Stomatal anatomical traits—including abaxial and adaxial density (D_{SAB}, D_{SAD}), length (L_{SAB}, L_{SAD}), and width (W_{SAB}, W_{SAD}) on both leaf surfaces, were not correlated with stomatal regulation traits, and only W_{SAB} was related to SSM (Figure S5).

4 | Discussion

In this study, we examined how the coordination between xylem structure and stomatal regulation determines hydraulic safety in the herbaceous crop species *Brassica oleracea* based on 2-month-old individuals from two contrasting grandparent lines (the large-leaved woody JKC and small-leaved herbaceous TO1000) and five of the resulting F2 genotypes. We found that the 1 MPa variation in stem P_{50} among the genotypes was best accounted for by intervessel pit membrane thickness (T_{PM}), followed by the vessel thickness-to-span ratio (T_{VW}/D_{MAX}). Despite the pronounced differences in pre-drought stomatal conductance ($g_{s\Psi 0}$) (3.6-fold), leaf size and total leaf area (3.5- and 24.6-fold, respectively), drought-induced stomatal behaviour was remarkably similar across genotypes, showing that the width of the positive SSM is largely determined by P_{50}.

4.1 | Intraspecific Variability in Cabbage Stem P_{50} Is Mainly Driven by the Intervessel Pit Membrane Thickness

Based on the optical vulnerability technique measured at the base of the stems, we observed a significant 1 MPa difference

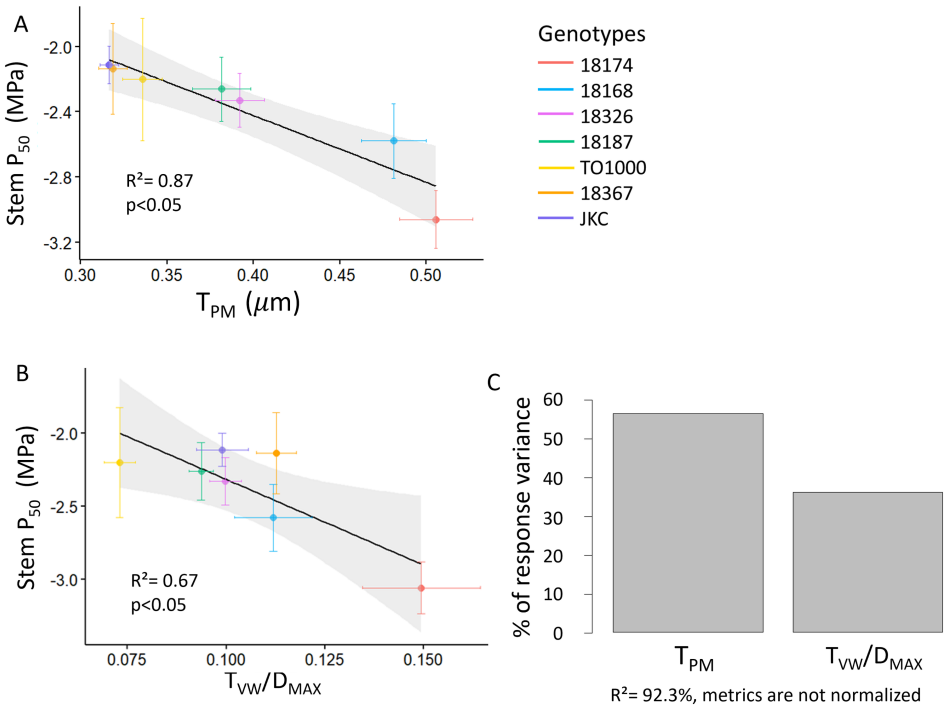

FIGURE 4 | Linear regression and relative importance of intervessel pit membrane thickness (T_{PM}) and thickness to span ratio of vessels (T_{VW}/D_{MAX}) to stem P_{50}. (A) Linear regression of T_{PM} and P_{50}. (B) Linear regression of T_{VW}/D_{MAX} and P_{50}. Each dot represents the average per genotype, and the bars represent the standard error (P_{50}, $n = 3$–4; T_{VW}/D_{MAX}, $n = 3$–5). (C) The relative importance of P_{50} variation is mainly explained by T_{PM} and T_{VW}/D_{MAX}, based on R^2 contribution averaged over orderings among regressors and determined using the Lindemann, Merenda, and Gold method. The R^2 and the p-values are given. Model parameters for P_{50}, P_{12}, and P_{88} are shown in Tables S2–S4.

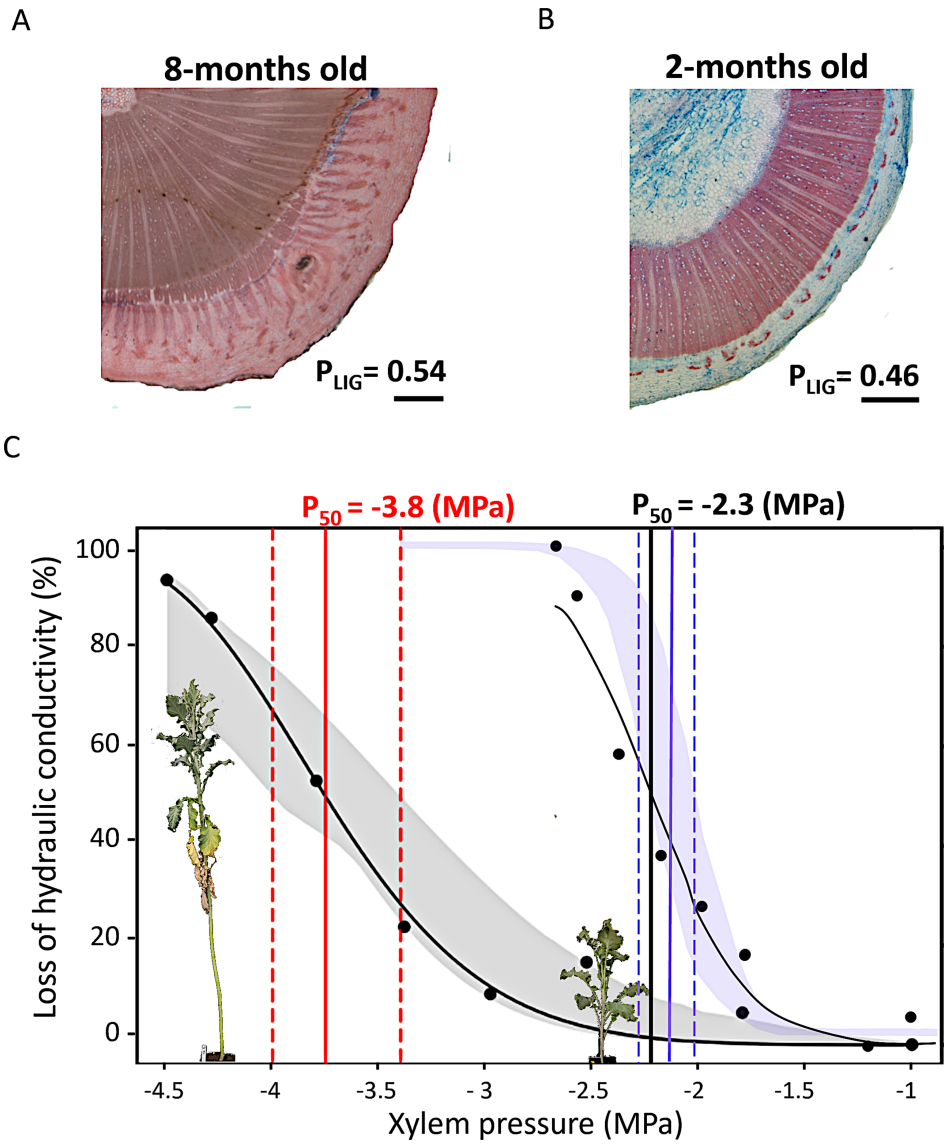

FIGURE 5 | P_{LIG}, stem sections and P_{50} of JKC genotype. (A) Cross-section of the basal stem part of an 8-month-old individual, P_{LIG} $n = 1$. (B) Cross-section of the basal stem part of a 2-month-old individual, P_{LIG} $n = 4$. Scale bars = 1000 μm. (C) Stem vulnerability curves for the JKC genotype at two developmental stages. For 2-month-old plants, P_{50} is indicated by a vertical black solid line (Cavitron method, $n = 1$) and a vertical purple solid line (OV method, $n = 4$); 95% confidence interval is shown as purple shading for the curve and purple dashed vertical lines for the P_{50}. For 8-month-old plants, P_{50} is indicated by a vertical red solid line ($n = 1$), with the 95% confidence interval shown as grey shading for the curve and red dashed vertical lines for the P_{50} computed using bootstrapping.

in P_{50} between the most resistant *B. oleracea* genotype (18174, P_{50}: −3.06 MPa) and the most sensitive one (grandparental line JKC, P_{50}: −2.11 MPa; Figure 1; Table 2). This difference is notable and suggests that even closely related genotypes can display distinct hydraulic strategies to cope with water deficit, which are functionally linked to anatomical traits, as our subsequent analyses indicate. These findings align with the broader pattern of within-species variation in P_{50} reported in other plants associated with contrasting environments or anatomical differences (López et al. 2016; Volaire et al. 2018; Dória et al. 2019; Ahmad et al. 2018; Thonglim et al. 2023). Our optical vulnerability results were consistent with stem P_{50} values obtained using the Cavitron centrifuge for a subset of genotypes (18187, 18326, JKC, and TO1000; Figure S4) and demonstrate that cabbage is a comparatively hydraulically vulnerable herbaceous crop. The stem P_{50} values measured here lie at the sensitive end of those reported for herbaceous Brassicaceae (−1.58 to −4.9 MPa; Dória et al. 2019; Thonglim et al. 2023) and are substantially less negative than values reported for many other herbaceous species, particularly grasses, which can tolerate much lower water potentials (down to −7.5 MPa; Lens et al. 2016; Volaire et al. 2018).

Among all the traits we measured, intervessel pit membrane thickness (T_{PM}) emerged as the strongest predictor for the variation in P_{50} (Figures 3V-AB, 4 and S6N, Table S2). This is consistent with growing evidence showing that angiosperm species tolerant to drought-induced embolism have thicker intervessel pit membranes (Lens et al. 2011, 2022; Li et al. 2016; Dória et al. 2018, 2019; Thonglim et al. 2021, 2023; Isasa et al. 2023). Furthermore, T_{PM} shows a stronger association with P_{88} (100%) and P_{50} (56.3%) than with P_{12} (19.5%), suggesting that T_{PM} becomes increasingly important as embolism

propagation progresses. While the exact nanoscale triggers of the onset of embolism in the xylem sap continue to be refined (Schenk et al. 2015; Zhang et al. 2020, 2024; Kaack et al. 2021; Lens et al. 2022), our findings align with the mechanistic intervessel pit models proposed by Kaack et al. (2019, 2021) and Zhang et al. (2020). Thicker pit membranes provide superior hydraulic safety because their 3D ultrastructure contains more tortuous, longer, and narrower multiconstriction pathways. This nanoscale architecture increases the physical resistance to the meniscus movement of air, thereby reducing the probability of air entrance at the pit level and the subsequent spread of embolism throughout the 3D vessel network (Jansen et al. 2009; Li et al. 2016; Kaack et al. 2019, 2021; Zhang et al. 2020; Lens et al. 2022).

4.2 | Beyond Pit Membranes: Correlation of Anatomical Traits and Their Contribution to Embolism Tolerance in *B. oleracea* Genotypes

In addition to T_{PM}, the ratio of double vessel wall thickness to vessel diameter (T_{VW}/D_{MAX}) was a good predictor of P_{50} and P_{12}. T_{VW}/D_{MAX} also contributed to most of the variation in the P_{12} model (48.8%), followed by fibre wall thickness (A_{FW}, 29.2%). The ratio of vessel wall thickness to vessel diameter (T_{VW}/D_{MAX}) was also significantly correlated with vessel wall thickness (T_V) ($R = 0.87$, $p < 0.05$). The maximum vessel lumen diameter (D_{MAX}), however, showed no correlation to traits that are associated with the hydraulic traits measured, such as intervessel pit membrane thickness or vessel or fibre wall thickness, implying that the functional signal in the T_{VW}/D_{MAX} versus P_{50} is determined by vessel wall thickening rather than changes in lumen size, as confirmed by Thonglim et al. (2021) and Bouché et al. (2014). The strong correlations between xylem cell wall thickening (T_V, T_{VW}/D_{MAX}, and A_{FW}) and hydraulic safety thresholds likely reflect a functional coordination rather than a direct causal link. Increased wall reinforcement and higher thickness-to-span ratios are best interpreted as mechanical consequences of a safer hydraulic strategy. Genotypes that resist the onset of embolism (P_{12}) and maintain conductivity at more negative pressures (P_{50}) must operate under higher xylem tension. Consequently, they require greater structural reinforcement to prevent conduit implosion as water potential drops toward these critical thresholds (Hacke et al. 2001). While ultrastructural properties of intervessel pit membranes serve as the mechanistic cause of embolism resistance by providing tortuous multiconstriction pathways that impede embolism spread across adjacent conduits (Kaack et al. 2021; Zhang et al. 2020), the vessel and fiber walls ensure the mechanical integrity required to reach those pressures without structural failure. This suggests that in *Brassica*, selection for drought tolerance has necessitated a simultaneous investment in both the nanoscale 'valves' (pit membranes) and the macroscale 'piping' (wall thickness).

Among other pit membrane traits, the chamber depth (D_{PC}) was not correlated with P_{50}, P_{12}, or P_{88}, nor was it retained in any of the multiple regression models, as previously reported for Brassicaceae (Thonglim et al. 2021; Dória et al. 2018). A notable anatomical feature in the pit chambers of the *Brassica* genotypes observed, and by extension in all members of the family Brassicaceae (Jansen et al. 2001), is the presence of vestures across all seven genotypes (Figure 3V-AB). These lignified cell wall projections are proposed to enhance hydraulic safety by providing mechanical support to the intervessel pit membrane, limiting its deflection and stretching under high xylem pressure gradients among adjacent conduits (Choat et al. 2004). As vestures were not quantified in detail in this study, our observations of the TEM images did not reveal any obvious variation in the level of vestured pits across the genotypes, therefore questioning their role in fine-tuning P_{50} and other hydraulic thresholds alongside pit membrane thickness.

Stem woodiness or lignification, expressed as the proportion of lignified area per total stem area (P_{LIG}), is a trait that has been associated with increased drought tolerance in predominantly herbaceous lineages and is often correlated with P_{50} and intervessel pit membrane characteristics (Lens et al. 2016; Dória et al. 2018, 2019; Thonglim et al. 2021; Thonglim et al. 2023; Zizka et al. 2022; Haverroth et al. 2024). However, in the *Brassica* genotypes investigated, P_{LIG} was not correlated with P_{50} nor with intervessel pit membrane thickness. Nevertheless, the associations we observed between P_{50} and P_{12} with T_{VW}/D_{MAX}, and between P_{12} and A_{FW}, suggest that embolism tolerance is related to thicker walls in both vessels and fibres, possibly reflecting higher levels of lignification at the cellular rather than the tissue level.

Although stem P_{50} is largely determined by stem xylem anatomical traits, water potential decline under drought propagates throughout the whole plant, and coordination between leaf traits and stem xylem vulnerability might therefore be expected. Indeed, several studies (Scoffoni et al. 2011; Nardini et al. 2014; Kröber et al. 2014; Guillemot et al. 2022; Schreiber et al. 2016) report associations between more negative P_{50} values and smaller leaves. However, we found no relationship between P_{50} and either total leaf area or individual leaf size, suggesting an uncoupling between leaf morphometry and stem vulnerability in these genotypes, potentially due to hydraulic segmentation between stem and leaves. This hypothesis could not be further evaluated, as leaf vulnerability could not be assessed with the Optical Vulnerability method, as the thickness of the midrib and leaf blade prevented the visualisation of embolism formation.

4.3 | Similarities and Differences in Strategies Showing the Interplay Between Stomatal Behaviour and Stem Hydraulics

Under pre-drought conditions, stomatal conductance ($g_{s\Psi 0}$) varied considerably among the seven genotypes (Figure 2; Table 2), with genotype 18174 exhibiting the most conservative water-use strategy, as indicated by the lowest $g_{s\Psi 0}$ values, while the others had $g_{s\Psi 0}$ values that were doubled or even more. However, leaf and stomatal size and number, which also showed high variability, did not explain this difference in $g_{s\Psi 0}$ even when stomatal size and number have been associated and described as anatomical constraints for stomatal conductance (Franks and Beerling 2009; Sack and Buckley 2016) and leaf size has been cited as a determinant for photosynthetic activity and water use (Valencia et al. 2016; Wang et al. 2019).

Despite these differences in $g_{s\Psi 0}$ and leaf size, the xylem water potential inducing 90% reduction of stomatal conductance (Ψg_{s90}) was similar across genotypes and occurred early during drought conditions, suggesting comparable thresholds for early stomatal closure in response to declining water availability. This pattern agrees with the general findings in other herbaceous Brassicaceae (Thonglim et al. 2023) and across a wide range of herbaceous and woody lineages, where stomatal closure operates within a relatively conserved physiological range and typically occurs way before dramatic levels of embolism spread (Roman et al. 2015; Combe et al. 2016; Martin-StPaul et al. 2017). Another noteworthy finding regarding Ψg_{s90} was its correlation with T_{Leaf}, suggesting that plants with smaller leaf area tend to close their stomata earlier. This observation is consistent with Wang et al. (2019), who demonstrated that smaller leaves experience higher water loss, which could necessitate earlier stomatal closure to limit excessive water loss from transpiration. Contrarily, we did not find any correlation between stomatal size or density and Ψg_{s90}, even though smaller stomata are generally thought to respond more rapidly to drought stress (Drake et al. 2013; Caine et al. 2019, 2023).

In the *B. oleracea* genotypes studied, stomatal safety margins (SSMs: $\Psi g_{s90} - P_{50}$) were positive for all genotypes and primarily driven by the differences in P_{50} (Figure 2). For example, the widest SSM (1.82 MPa) occurred in genotype 18174, showing the most negative stem P_{50}. Although this genotype also exhibits the lowest stomatal conductance (see above), a larger SSM in herbaceous species does not necessarily confer higher drought survival (Haverroth et al. 2023; Pereira et al. 2024).

Overall, the *Brassica* genotypes displayed distinct strategies balancing water use and hydraulic safety. Some, such as 18174, combine low $g_{s\Psi 0}$ with a wide SSM and a more negative P_{50}, reflecting conservative water use and high hydraulic safety. Others, including 18168, JKC, and 18187, couple higher $g_{s\Psi 0}$ with narrower safety margins, potentially prioritising growth over drought tolerance. These findings at a two-month developmental stage provide initial insights into which genotypes may be more drought-tolerant. Future studies should therefore assess drought tolerance under controlled drought experiments while standardising leaf size (or accounting for leaf size effects) to enable robust and comparable evaluations across the genotypes. Furthermore, to dive deeper into the diversity of drought strategies across the *Brassica* genotypes studied, other traits need to be investigated, such as root depth, leaf turgor loss point and capacitance, and residual stomatal conductance (Chaves et al. 2003; Ilyas et al. 2021; Chen et al. 2022; Pereira et al. 2024), but that is beyond the scope of our study.

4.4 | Potential Age Effect on Woodiness and Vulnerability to Drought-Induced Embolism

Previous studies in other herbaceous species grown under controlled conditions, such as *Solanum lycopersicum* L. and *Senecio minimus* Poir., suggested that tolerance to drought-induced embolism in stems enhances with increased stem woodiness, either due to older plant age between individuals or due to older developmental age of the xylem at the stem base compared to distal later-formed parts (Lamarque et al. 2020; Haverroth et al. 2024). Although increased stem woodiness or lignification (P_{LIG}) was not correlated with P_{50} across the 2-month-old Brassica genotypes, we did observe a similar trend using a limited pilot experiment of the Jersey kale (JKC) genotype where the stem P_{50} of one woodier eight-month stem was considerably more negative than the average stem P_{50} from three 2-month-old, less woody JKC individuals (−3.8 MPa vs. −2.3 MPa and 54% vs. 46% P_{LIG}; Figure 5). A potential correlation between plant age, P_{LIG} and P_{50} in herbaceous species has been suggested as a potential mechanism to secure water supply to reproductive organs (Harrison Day et al. 2022; Haverroth et al. 2024). However, it needs to be assessed whether this suggested age–P_{LIG}–P_{50} effect in herbaceous plants leads to a stronger total plant drought tolerance with age, or whether the more negative stem P_{50} values in older stems merely counterbalance the increased water demand due to a larger canopy. Therefore, targeted drought experiments coupled with anatomical observations across developmental stages of multiple individuals from various species would provide a more dynamic perspective of drought tolerance throughout the life cycle of herbaceous species.

In conclusion, the seven 2-month-old *B. oleracea* genotypes exhibited contrasting water-use and hydraulic strategies under well-watered and drought conditions. Variations in pre-drought stomatal conductance ($g_{s\Psi 0}$) under non-limiting conditions revealed a spectrum from conservative to acquisitive water-use types. However, Ψg_{s90} values were similar across genotypes, showing comparable thresholds for stomatal closure. This indicates that differences in drought response among genotypes are not driven by the timing of stomatal closure, but rather by other traits not measured in our study (e.g., lower residual stomatal conductance, high capacitance pre- and post-turgor loss, osmotic adjustment, enhanced water uptake capacity (Chaves et al. 2003; Ilyas et al. 2021; Chen et al. 2022; Pereira et al. 2024)).

The SSMs were positive for all genotypes, confirming functional coordination between stomatal behaviour and xylem hydraulics, and primarily driven by variation in stem P_{50}. Tolerance to drought-induced embolism among the cabbage genotypes was best predicted by intervessel pit membrane thickness, not by stem woodiness in the 2-month-old genotypes. This implies that genotypes with thicker pit membranes have more negative stem P_{50} values and maintain greater hydraulic safety relative to stomatal closure, thereby reducing the risk of hydraulic failure during drought. In other words, genotypic differences in hydraulic safety arise from the interplay between conservative water-use behaviour and intrinsic xylem structural resistance, rather than from woodiness or earlier stomatal closure.

Author Contributions

N.A.P.-Z., G.B., and F.L.: conceptualization; N.A.P.-Z., R.B., J.v.H., M.v.U., K.W. and M.L.: carried out experiments; N.A.P.-Z., G.B., S.D. and M.L.: formal analysis; F.L. and S.B.: funding acquisition; N.A.P.-Z., G.B., S.D., R.B., M.L. and F.L.: methodology; S.D., S.B., and F.L.: resources; F.L., G.B. and S.B.: supervision; N.A.P.-Z. and F.L.: visualization and writing – original draft; N.A.P.-Z., G.B., S.D., M.L., R.B., S.B., and F.L.: writing – review and editing. All authors read and approved the final manuscript.

Acknowledgements

We thank Ellora Basu (IBL) for taking care of the tissue culture, Bertie Joan van Heuven and Rob Langelaan for their help with lab work at Naturalis (LM, TEM), Gaelle Capdeville (BIOGECO INRA) for training and technical support with the Cavitron centrifuge in Bordeaux, and three anonymous reviewers who contributed to improving the manuscript. The authors declare that no Generative AI tools were used to generate ideas, interpret results, generate or modify figures or alter the structure of this manuscript. Generative AI was exclusively used for grammar and language editing.

Funding

This work was funded by the Dutch Research Council NWO (OCENW.XL21.XL21.059).

Data Availability Statement

The data that supports the findings of this study are available in the supporting information of this article.

References

Ahmad, H. B., F. Lens, G. Capdeville, R. Burlett, L. J. Lamarque, and S. Delzon. 2018. "Intraspecific Variation in Embolism Resistance and Stem Anatomy Across Four Sunflower (*Helianthus annuus* L.) Accessions." *Physiologia Plantarum* 163: 59–72.

Alon, A., S. Cohen, R. Burlett, et al. 2024. "Leaf Membrane Leakage and Xylem Hydraulic Failure Define the Point of No Return in Drought-Induced Tree Mortality in *Cupressus sempervirens*." *Physiologia Plantarum* 176: 1–13.

Andrade, M. T., L. A. Oliveira, T. S. Pereira, et al. 2022. "Impaired Auxin Signaling Increases Vein and Stomatal Density but Reduces Hydraulic Efficiency and Ultimately Net Photosynthesis." *Journal of Experimental Botany* 73: 4147–4156.

Ayaz, F. A., R. H. Glew, M. Millson, et al. 2006. "Nutrient Contents of Kale (*Brassica oleracea* L. Var. *Acephala* DC.)." *Food Chemistry* 96: 572–579.

Ben Ammar, H., V. Picchi, D. Arena, et al. 2022. "Variation of Bio-Morphometric Traits and Antioxidant Compounds of *Brassica oleracea* L. Accessions in Relation to Drought Stress." *Agronomy* 12: 2016.

Benjamini, Y., and Y. Hochberg. 1995. "Controlling the False Discovery Rate: A Practical and Powerful Approach to Multiple Testing." *Journal of the Royal Statistical Society: Series B* 57: 289–300.

Bortolami, G., T. A. de Werk, M. Larter, et al. 2024. "Integrating Gene Expression Analysis and Ecophysiological Responses to Water Deficit in Leaves of Tomato Plants." *Scientific Reports* 14: 1–12.

Bouché, P. S., M. Larter, J. C. Domec, et al. 2014. "A Broad Survey of Hydraulic and Mechanical Safety in the Xylem of Conifers." *Journal of Experimental Botany* 65: 4419–4431.

Brodribb, T. J., C. R. Brodersen, M. Carriqui, et al. 2021. "Linking Xylem Network Failure With Leaf Tissue Death." *New Phytologist* 232: 68–79.

Brodribb, T. J., M. Carriqui, S. Delzon, and C. Lucani. 2017. "Optical Measurement of Stem Xylem Vulnerability." *Plant Physiology* 174: 2054–2061.

Brodribb, T. J., and R. S. Hill. 1999. "The Importance of Xylem Constraints in the Distribution of Conifer Species." *New Phytologist* 143: 365–372.

Brodribb, T. J., R. P. Skelton, S. A. M. McAdam, D. Bienaimé, C. J. Lucani, and P. Marmottant. 2016. "Visual Quantification of Embolism Reveals Leaf Vulnerability to Hydraulic Failure." *New Phytologist* 209: 1403–1409.

Caine, R. S., E. L. Harrison, J. Sloan, et al. 2023. "The Influences of Stomatal Size and Density on Rice Abiotic Stress Resilience." *New Phytologist* 237: 2180–2195.

Caine, R. S., X. Yin, J. Sloan, et al. 2019. "Rice With Reduced Stomatal Density Conserves Water and Has Improved Drought Tolerance Under Future Climate Conditions." *New Phytologist* 221: 371–384.

Chaves, M. M., J. P. Maroco, and J. S. Pereira. 2003. "Understanding Plant Responses to Drought—From Genes to the Whole Plant." *Functional Plant Biology* 30: 239–264.

Chen, Z., S. Li, X. Wan, and S. Liu. 2022. "Strategies of Tree Species to Adapt to Drought From Leaf Stomatal Regulation and Stem Embolism Resistance to Root Properties." *Frontiers in Plant Science* 13: 926535.

Choat, B., S. Jansen, T. J. Brodribb, et al. 2012. "Global Convergence in the Vulnerability of Forests to Drought." *Nature* 491: 752–755.

Choat, B., S. Jansen, M. A. Zwieniecki, E. Smets, and N. M. Holbrook. 2004. "Changes in Pit Membrane Porosity due to Deflection and Stretching: The Role of Vestured Pits." *Journal of Experimental Botany* 55: 1569–1575.

Cochard, H. 2002a. "Xylem Embolism and Drought-Induced Stomatal Closure in Maize." *Planta* 215: 466–471.

Cochard, H. 2002b. "A Technique for Measuring Xylem Hydraulic Conductance Under High Negative Pressures." *Plant, Cell & Environment* 25: 815–819.

Cochard, H., G. Damour, C. Bodet, I. Tharwat, M. Poirier, and T. Améglio. 2005. "Evaluation of a New Centrifuge Technique for Rapid Generation of Xylem Vulnerability Curves." *Physiologia Plantarum* 124: 410–418.

Combe, M., J. V. G. de Arellano, H. G. Ouwersloot, and W. Peters. 2016. "Plant Water-Stress Parameterization Determines the Strength of Land–Atmosphere Coupling." *Agricultural and Forest Meteorology* 217: 61–73.

Dayer, S., J. C. Herrera, Z. Dai, et al. 2020. "The Sequence and Thresholds of Leaf Hydraulic Traits Underlying Grapevine Varietal Differences in Drought Tolerance." *Journal of Experimental Botany* 71: 4333–4344.

Dória, L. C., C. Meijs, D. S. Podadera, et al. 2019. "Embolism Resistance in Stems of Herbaceous Brassicaceae and Asteraceae Is Linked to Differences in Woodiness and Precipitation." *Annals of Botany* 124: 1–14.

Dória, L. C., D. S. Podadera, M. del Arco, et al. 2018. "Insular Woody Daisies (*Argyranthemum*, Asteraceae) Are More Resistant to Drought-Induced Hydraulic Failure Than Their Herbaceous Relatives." *Functional Ecology* 32: 1467–1478.

Drake, P. L., R. H. Froend, and P. J. Franks. 2013. "Smaller, Faster Stomata: Scaling of Stomatal Size, Rate of Response and Stomatal Conductance." *Journal of Experimental Botany* 64: 495–505.

FAO. 2023. FAOSTAT—Worldwide Production and Yield of Cabbage, Cauliflower and Broccoli Accessed 20 November 2024. https://www.fao.org/faostat/en/#data/QCL.

Franks, P. J., and D. J. Beerling. 2009. "Maximum Leaf Conductance Driven by CO_2 Effects on Stomatal Size and Density Over Geologic Time." *Proceedings of the National Academy of Sciences of the United States of America* 106: 10343–10347.

Garcia, M. N., T. F. Domingues, R. S. Oliveira, and F. R. C. Costa. 2023. "The Biogeography of Embolism Resistance Across Resource Gradients in the Amazon." *Global Ecology and Biogeography* 32: 2199–2211.

Ghosh, A., A. Kumar, and G. Biswas. 2024. "Exponential Population Growth and Global Food Security: Challenges and Alternatives." In *Bioremediation of Emerging Contaminants From Soils*, edited by P. Kumar, A. L. Srivastav, V. Chaudhary, et al., 1–20. Elsevier.

Grigorieva, E., A. Livenets, and E. Stelmakh. 2023. "Adaptation of Agriculture to Climate Change: A Scoping Review." *Climate* 11: 202.

Guillemot, J., N. K. Martin-StPaul, L. Bulascoschi, et al. 2022. "Small and Slow Is Safe: On the Drought Tolerance of Tropical Tree Species." *Global Change Biology* 28: 2622–2638.

Hacke, U. G., J. S. Sperry, W. T. Pockman, S. D. Davis, and K. A. McCulloh. 2001. "Trends in Wood Density and Structure Are Linked to Prevention of Xylem Implosion by Negative Pressure." *Oecologia* 126: 457–461.

Hammond, W. M., K. Yu, L. A. Wilson, R. E. Will, W. R. L. Anderegg, and H. D. Adams. 2019. "Dead or Dying? Quantifying the Point of no Return From Hydraulic Failure in Drought-Induced Tree Mortality." *New Phytologist* 223: 1834–1843.

Harrison Day, B. L., and T. J. Brodribb. 2023. "Resistant Xylem From Roots to Peduncles Sustains Reproductive Water Supply After Drought-Induced Cavitation of Wheat Leaves." *Annals of Botany* 131: 839–850.

Harrison Day, B. L., M. R. Carins-Murphy, and T. J. Brodribb. 2022. "Reproductive Water Supply Is Prioritized During Drought in Tomato." *Plant, Cell & Environment* 45: 69–79.

Harrison Day, B. L., K. M. Johnson, V. Tonet, et al. 2023. "The Root of the Problem: Diverse Vulnerability to Xylem Cavitation Within the Root System of Wheat Plants." *New Phytologist* 239: 1239–1252.

Haverroth, E. J., L. A. Oliveira, M. T. Andrade, et al. 2023. "Abscisic Acid Acts Essentially on Stomata, Not on Xylem, to Improve Drought Resistance in Tomato." *Plant, Cell & Environment* 46: 3229–3241.

Haverroth, E. J., I. M. Rimer, L. A. Oliveira, et al. 2024. "Gradients in Embolism Resistance Within Stems Driven by Secondary Growth in Herbs." *Plant, Cell & Environment* 47: 2986–2998.

Hilu, K. W., and J. L. Randall, 1984. "Convenient Method for Studying Grass Leaf Epidermis." *Taxon* 33: 413–415.

Huang, R., N. Di, B. Xi, et al. 2024. "Herb Hydraulics: Variation and Correlation for Traits Governing Drought Tolerance and Efficiency of Water Transport." *Science of the Total Environment* 907: 168095.

Ilyas, M., M. Nisar, N. Khan, et al. 2021. "Drought Tolerance Strategies in Plants: A Mechanistic Approach." *Journal of Plant Growth Regulation* 40: 926–944.

Isasa, E., R. M. Link, S. Jansen, et al. 2023. "Addressing Controversies in the Xylem Embolism Resistance–Vessel Diameter Relationship." *New Phytologist* 238: 283–296.

Jansen, S., P. Baas, and E. Smets. 2001. "Vestured Pits: Their Occurrence and Systematic Importance in Eudicots." *Taxon* 50: 135–167.

Jansen, S., B. Choat, and A. Pletsers. 2009. "Morphological Variation of Intervessel Pit Membranes and Implications for Xylem Function in Angiosperms." *American Journal of Botany* 96: 409–419.

Kaack, L., C. M. Altaner, C. Carmesin, et al. 2019. "Function and Three-Dimensional Structure of Intervessel Pit Membranes in Angiosperms: A Review." *IAWA Journal* 40: 673–702.

Kaack, L., M. Weber, E. Isasa, et al. 2021. "Pore Constrictions in Intervessel Pit Membranes Provide a Mechanistic Explanation for Xylem Embolism Resistance in Angiosperms." *New Phytologist* 230: 1829–1843.

Karnovsky, M. J. 1965. "A Formaldehyde–Glutaraldehyde Fixative of High Osmolality for Use in Electron Microscopy." *Journal of Cell Biology* 27: 137–138A.

Kidner, C., A. Groover, D. Thomas, et al. 2016. "First Steps in Studying the Origins of Secondary Woodiness in Begonia (B Egoniaceae): Combining Anatomy, Phylogenetics, and Stem Transcriptomics." *Biological Journal of the Linnean Society* 117: 121–138.

Kolb, K. J., and J. S. Sperry. 1999. "Differences in Drought Adaptation Between Subspecies of Sagebrush (*Artemisia tridentata*)." *Ecology* 80: 2373–2384.

Kröber, W., S. Zhang, M. Ehmig, and H. Bruelheide. 2014. "Linking Xylem Hydraulic Conductivity and Vulnerability to the Leaf Economics Spectrum—A Cross-Species Study of 39 Evergreen and Deciduous Broadleaved Subtropical Tree Species." *PLoS One* 9: e109211.

Lamarque, L. J., S. Delzon, H. Toups, et al. 2020. "Over-Accumulation of Abscisic Acid in Transgenic Tomato Plants Increases the Risk of Hydraulic Failure." *Plant, Cell & Environment* 43: 548–562.

Larter, M., S. Pfautsch, J. C. Domec, S. Trueba, N. Nagalingum, and S. Delzon. 2017. "Aridity Drove the Evolution of Extreme Embolism Resistance and the Radiation of Conifer Genus *Callitris*." *New Phytologist* 215: 97–112.

Lens, F., S. Dressler, S. Jansen, L. van Evelghem, and E. Smets. 2005. "Relationships Within Balsaminoid Ericales: A Wood Anatomical Approach." *American Journal of Botany* 92: 941–953.

Lens, F., S. Eeckhout, R. Zwartjes, E. Smets, and S. B. Janssens. 2012. "The Multiple Fuzzy Origins of Woodiness Within Balsaminaceae Using an Integrated Approach. Where Do We Draw the Line?" *Annals of Botany* 109: 783–799.

Lens, F., S. M. Gleason, G. Bortolami, C. Brodersen, S. Delzon, and S. Jansen. 2022. "Functional Xylem Characteristics Associated With Drought-Induced Embolism in Angiosperms." *New Phytologist* 236: 2019–2036.

Lens, F., S. M. Gleason, G. Bortolami, et al. 2023. "Comparative Anatomy vs. Mechanistic Understanding: How to Interpret the Diameter-Vulnerability Link." *IAWA Journal* 44: 368–380.

Lens, F., C. Picon-Cochard, C. E. L. Delmas, et al. 2016. "Herbaceous Angiosperms Are Not More Vulnerable to Drought-Induced Embolism Than Angiosperm Trees." *Plant Physiology* 172: 661–667.

Lens, F., J. S. Sperry, M. A. Christman, B. Choat, D. Rabaey, and S. Jansen. 2011. "Testing Hypotheses That Link Wood Anatomy to Cavitation Resistance and Hydraulic Conductivity in the Genus *Acer*." *New Phytologist* 190: 709–723.

Lens, F., A. Tixier, H. Cochard, J. S. Sperry, S. Jansen, and S. Herbette. 2013. "Embolism Resistance as a Key Mechanism to Understand Adaptive Plant Strategies." *Current Opinion in Plant Biology* 16: 287–292.

Lenth, R., H. Singmann, J. Love, et al. 2018. *emmeans*: Estimated Marginal Means. R Package Version 4.0-3.

Li, S., F. Lens, S. Espino, et al. 2016. "Intervessel Pit Membrane Thickness as a Key Determinant of Embolism Resistance in Angiosperm Xylem." *IAWA Journal* 37: 152–171.

Li, Y., J. S. Sperry, and M. Shao. 2009. "Hydraulic Conductance and Vulnerability to Cavitation in Corn (*Zea mays* L.) Hybrids of Differing Drought Resistance." *Environmental and Experimental Botany* 66: 341–346.

Lindeman, R. H., P. F. Merenda, and R. Z. Gold. 1980. *Introduction to Bivariate and Multivariate Analysis* (Vol. 4), 119. Scott, Foresman.

López, R., F. J. Cano, B. Choat, et al. 2016. "Plasticity in Vulnerability to Cavitation of *Pinus canariensis* Occurs Only at the Driest End of an Aridity Gradient." *Frontiers in Plant Science* 7: 1–10.

Mafakheri, M., and M. Kordrostami. 2020. "Newly Revealed Promising Gene Pools of Neglected Brassica Species to Improve Stress-Tolerant Crops." In *The Plant Family Brassicaceae*, edited by M. Hasanuzzaman, 181–193. Springer.

Maherali, H., W. T. Pockman, and R. B. Jackson. 2004. "Adaptive Variation in the Vulnerability of Woody Plants to Xylem Cavitation." *Ecology* 85: 2184–2199.

Mantova, M., H. Cochard, R. Burlett, et al. 2023. "On the Path From Xylem Hydraulic Failure to Downstream Cell Death." *New Phytologist* 237: 793–806.

Mantova, M., S. Herbette, H. Cochard, and T. Ruiz. 2022. "Hydraulic Failure and Tree Mortality: From Correlation to Causation." *Trends in Plant Science* 27: 335–345.

Mantova, M., P. E. Menezes-Silva, E. Badel, H. Cochard, and J. M. Torres-Ruiz. 2021. "The Interplay of Hydraulic Failure and Cell Vitality Explains Tree Capacity to Recover From Drought." *Physiologia Plantarum* 172: 247–257.

Martin-StPaul, N., S. Delzon, and H. Cochard. 2017. "Plant Resistance to Drought Depends on Timely Stomatal Closure." *Ecology Letters* 20: 1437–1447.

Max, A. C., L. Loram-Lourenço, F. G. Silva, et al. 2023. "A Bitter Future for Coffee Production? Physiological Traits Associated With Yield Reveal High Vulnerability to Hydraulic Failure in *Coffea canephora*." *Plant, Cell & Environment* 46: 764–779.

McDowell, N. G., W. T. Pockman, C. D. Allen, et al. 2008. "Mechanisms of Plant Survival and Mortality During Drought: Why Do Some Plants Survive While Others Succumb to Drought?" *New Phytologist* 178: 719–739.

McDowell, N. G., G. Sapes, A. Pivovaroff, et al. 2022. "Mechanisms of Woody-Plant Mortality Under Rising Drought, CO_2 and Vapour Pressure Deficit." *Nature Reviews Earth and Environment* 3: 294–308.

Meza, I., S. Siebert, P. Döll, et al. 2020. "Global-Scale Drought Risk Assessment for Agricultural Systems." *Natural Hazards and Earth System Sciences* 20: 695–712.

Nardini, A., E. Õunapuu-Pikas, and T. Savi. 2014. "When Smaller Is Better: Leaf Hydraulic Conductance and Drought Vulnerability Correlate to Leaf Size and Venation Density Across Four *Coffea arabica* Genotypes." *Functional Plant Biology* 41: 972–982.

Pammenter, N. W., and C. Vander Willigen. 1998. "A Mathematical and Statistical Analysis of the Curves Illustrating Vulnerability of Xylem to Cavitation." *Tree Physiology* 18: 589–593.

Parker, S., and G. Stevens-Cox. 1970. *The Giant Cabbage of the Channel Islands*. Vol. 10. Guernsey Historical Monograph.

Parkin, I. A., C. Koh, H. Tang, et al. 2014. "Transcriptome and Methylome Profiling Reveals Relics of Genome Dominance in the Mesopolyploid *Brassica oleracea*." *Genome Biology* 15: 1–18.

Pereira, L., A. P. Domingues-Junior, S. Jansen, B. Choat, and P. Mazzafera. 2018. "Is Embolism Resistance in Plant Xylem Associated With Quantity and Characteristics of Lignin?" *Trees* 32: 349–358.

Pereira, T. S., L. A. Oliveira, M. T. Andrade, et al. 2024. "Linking Water-Use Strategies With Drought Resistance Across Herbaceous Crops." *Physiologia Plantarum* 176: 1–12.

PhenoBois. 2026. *OpenOV_AutoScan [Computer Software]*. GitLab Université de Bordeaux. https://gitub.u-bordeaux.fr/phenobois/ope-nov_autoscan.

Pinheiro, J. 2011. nlme: Linear and Nonlinear Mixed Effects Models. R Package.

Pivovaroff, A. L., V. M. W. Cook, and L. S. Santiago. 2018. "Stomatal Behaviour and Stem Xylem Traits Are Coordinated for Woody Plant Species Under Exceptional Drought Conditions." *Plant, Cell and Environment* 41: 2617–2626.

Rakow, G. 2004. "Species Origin and Economic Importance of *Brassica*." In *Brassica*, edited by E. Pua and C. Douglas, 3–11. Springer.

Razouk, R., L. Hssaini, M. Alghoum, A. Adiba, and A. Hamdani. 2022. "Phenotyping Olive Cultivars for Drought Tolerance Using Leaf Macro-Characteristics." *Horticulturae* 8: 939.

Roman, D. T., K. A. Novick, E. R. Brzostek, D. Dragoni, F. Rahman, and R. P. Phillips. 2015. "The Role of Isohydric and Anisohydric Species in Determining Ecosystem-Scale Response to Severe Drought." *Oecologia* 179: 641–654.

Sack, L., and T. N. Buckley. 2016. "The Developmental Basis of Stomatal Density and Flux." *Plant Physiology* 171: 2358–2363.

Sahin, U., M. Ekinci, S. Ors, M. Turan, S. Yildiz, and E. Yildirim. 2018. "Effects of Individual and Combined Effects of Salinity and Drought on Physiological, Nutritional and Biochemical Properties of Cabbage (*Brassica oleracea var. capitata*)." *Scientia Horticulturae* 240: 196–204.

Schenk, H. J., K. Steppe, and S. Jansen. 2015. "Nanobubbles: A New Paradigm for Air-Seeding in Xylem." *Trends in Plant Science* 20: 199–205.

Schindelin, J., I. Arganda-Carreras, E. Frise, et al. 2012. "Fiji: An Open-Source Platform for Biological-Image Analysis." *Nature Methods* 9: 676–682.

Schönbeck, L., C. Grossiord, A. Gessler, et al. 2022. "Photosynthetic Acclimation and Sensitivity to Short-and Long-Term Environmental Changes in a Drought-Prone Forest." *Journal of Experimental Botany* 73: 2576–2588.

Schreiber, S. G., U. G. Hacke, S. Chamberland, et al. 2016. "Leaf Size Serves as a Proxy for Xylem Vulnerability to Cavitation in Plantation Trees." *Plant, Cell and Environment* 39: 272–281.

Schuldt, B., F. Knutzen, S. Delzon, et al. 2016. "How Adaptable Is the Hydraulic System of European Beech in the Face of Climate Change-Related Precipitation Reduction?" *New Phytologist* 210: 443–458.

Scoffoni, C., M. Rawls, A. McKown, H. Cochard, and L. Sack. 2011. "Decline of Leaf Hydraulic Conductance With Dehydration: Relationship to Leaf Size and Venation Architecture." *Plant Physiology* 156: 832–843.

Searle, S. R., F. M. Speed, and G. A. Milliken. 1980. "Population Marginal Means in the Linear Model: An Alternative to Least Squares Means." *American Statistician* 34: 216–221.

Singh, J., A. K. Upadhyay, K. Prasad, A. Bahadur, and M. Rai. 2007. "Variability of Carotenes, Vitamin C, E and Phenolics in *Brassica* Vegetables." *Journal of Food Composition and Analysis* 20: 106–112.

Skelton, R. P., T. J. Brodribb, and B. Choat. 2017. "Casting Light on Xylem Vulnerability in an Herbaceous Species Reveals a Lack of Segmentation." *New Phytologist* 214: 561–569.

Skelton, R. P., A. G. West, and T. E. Dawson. 2015. "Predicting Plant Vulnerability to Drought in Biodiverse Regions Using Functional Traits." *PNAS* 112: 5744–5749.

Stoewsand, G. S. 1995. "Bioactive Organosulfur Phytochemicals in *Brassica oleracea* Vegetables—A Review." *Food and Chemical Toxicology* 33: 537–543.

Thonglim, A., G. Bortolami, S. Delzon, et al. 2023. "Drought Response in *Arabidopsis* Displays Synergistic Coordination Between Stems and Leaves." *Journal of Experimental Botany* 74: 1004–1021.

Thonglim, A., S. Delzon, M. Larter, et al. 2021. "Intervessel Pit Membrane Thickness Best Explains Variation in Embolism Resistance Amongst Stems of *Arabidopsis thaliana* Accessions." *Annals of Botany* 128: 171–182.

Torres-Ruiz, J. M., H. Cochard, S. Delzon, et al. 2024. "Plant Hydraulics at the Heart of Plant, Crops and Ecosystem Functions in the Face of Climate Change." *New Phytologist* 241: 984–999.

Tyree, M. T., and J. S. Sperry. 1989. "Vulnerability of Xylem to Cavitation and Embolism." *Annual Review of Plant Physiology and Plant Molecular Biology* 40: 19–36.

Tyree, M. T., and M. H. Zimmermann. 2013. *Xylem Structure and the Ascent of Sap*. Springer.

Urli, M., A. J. Porté, H. Cochard, et al. 2013. "Xylem Embolism Threshold for Catastrophic Failure in Angiosperm Trees." *Tree Physiology* 33: 672–683.

Valencia, E., J. L. Quero, and F. T. Maestre. 2016. "Functional Leaf and Size Traits Determine the Photosynthetic Response of 10 Dryland Species to Warming." *Journal of Plant Ecology* 9: 773–783.

van Haasteren, J., M. Larter, and F. Lens. 2019. Response to Drought of a Giant Woody Cabbage Cross. MSc Thesis, Leiden University, Leiden, The Netherlands.

Volaire, F., F. Lens, H. Cochard, et al. 2018. "Embolism and Mechanical Resistances Play a Key Role in Dehydration Tolerance of a Perennial Grass *Dactylis glomerata* L." *Annals of Botany* 122: 325–336.

Vos, R. A., C. A. M. van der Veen-van Wijk, M. E. Schranz, et al. 2022. "Refining Bulk Segregant Analyses: Ontology-Mediated Discovery of Flowering Time Genes in *Brassica oleracea*." *Plant Methods* 18: 1–11.

Wang, C., J. He, T. H. Zhao, et al. 2019. "The Smaller the Leaf Is, the Faster the Leaf Water Loses in a Temperate Forest." *Frontiers in Plant Science* 10: 58.

Wright, I. J., N. Dong, V. Maire, et al. 2017. "Global Climatic Drivers of Leaf Size." *Science* 357: 917–921.

Yates, M. J., G. Anthony Verboom, A. G. Rebelo, and M. D. Cramer. 2010. "Ecophysiological Significance of Leaf Size Variation in Proteaceae From the Cape Floristic Region." *Functional Ecology* 24: 485–492.

Yuan, X., Y. Wang, P. Ji, P. Wu, J. Sheffield, and J. A. Otkin. 2023. "A Global Transition to Flash Droughts Under Climate Change." *Science* 380: 187–191.

Zhang, Y., C. Carmesin, L. Kaack, et al. 2020. "High Porosity With Tiny Pore Constrictions and Unbending Pathways Characterize the 3D Structure of Intervessel Pit Membranes in Angiosperm Xylem." *Plant, Cell and Environment* 43: 116–130.

Zhang, Y., L. Pereira, L. Kaack, J. Liu, and S. Jansen. 2024. "Gold Perfusion Experiments Support the Multi-Layered, Mesoporous Nature of Intervessel Pit Membranes in Angiosperm Xylem." *New Phytologist* 242: 493–506.

Zizka, A., R. E. Onstein, R. Rozzi, et al. 2022. "The Evolution of Insular Woodiness." *Proceedings of the National Academy of Sciences of the United States of America* 119: 1–11.

Supporting Information

Additional supporting information can be found online in the Supporting Information section. **Table S1:** Mean values and standard error for all the traits measured in the seven *B. oleracea* genotypes, ranging from most to least embolism resistant, $n = 3–5$. Abbreviations follow Table 1. **Table S2:** Most parsimonious significant multiple linear regression model (AIC = −6.43) of stem anatomical variables indicate that T_{PM} and T_{VW}/D_{MAX}, to a lesser extent, account for P_{50} variation among the seven *B. oleracea* genotypes ($F = 24$, $R^2 = 0.92$, $p = 0.006$). *p-value < 0.05. **Table S3:** Most parsimonious significant multiple linear regression model (AIC = −11.07) of stem anatomical variables show that T_{VW}/D_{MAX} and A_{FW}, together with T_{PM}, to a lesser extent, account for P_{12} variation among the seven *B. oleracea* genotypes ($F = 38.9$, $R^2 = 0.98$, $p = 0.007$). *p-value < 0.05. **Table S4:** Most parsimonious significant multiple linear regression model (AIC = 3.65) where T_{PM} account for P_{88} variation among the seven *B. oleracea* genotypes ($F = 16.6$, $R^2 = 0.77$, $p = 0.01$). *p value < 0.05. **Figure S1:** Results from leaf water potential and stomatal conductance decline during a pilot drought experiment (MSc thesis of van Haasteren et al. 2019), which was used as a guideline for the selection of the F2 genotypes analysed in this study. Stomatal conductance measurements were repeated throughout the drought experiment, with ~5 days between each set of measurements. Predawn leaf water potential measurements were performed during drought and midday leaf water potentials on the last day of drought. Linear regression fitting was calculated for each measurement, excluding the controls. The minimum represents the predawn measurements while the maximum represents the midday measurements. **Figure S2:** Experiment layout for the stem's xylem picture recording for the optical vulnerability method. Duct sealer clay was placed over the Epson flatbed scanner to contain the hydrogel where the stem was placed. **Figure S3:** Boxplots with linear mixed models pairwise comparison with estimated marginal means and Benjamini and Hochberg adjustment of gs of the well-watered and drought batches for each genotype at water potential ≤ -1, P_{50} and Ψg_{s90} per genotype. (A) Variation in stomatal conductance (gs) of control (Co) and drought (Dr) batches per genotype and among genotypes at water potential ≤ -1, (B) variation in embolism resistance (P50) among genotypes, and (C) variation in water potential at 90% of stomatal closure (Ψgs90). p-value < 0.05. **Figure S4:** Stem vulnerability curves obtained with the Cavitron centrifuge for genotypes 18187, 18326, JKC and TO1000. (A–D) 18187, (E–G) 18326, (H) JKC and (I) TO1000, used to estimate (J) the average vulnerability curves and (K) P_{50} values per genotype for this technique. **Figure S5:** Pearson's coefficients ($p < 0.05$) of the correlation of all the variables measured in this study. Abbreviations follow Table 1 ***p-value < 0.001; **p-value < 0.01; *p-value < 0.05. **Figure S6:** Boxplots with linear mixed models pairwise comparison with estimated marginal means and Benjamini and Hochberg adjustment of stem anatomical variables per genotype. Abbreviations follow Table 1. $p < 0.05$. **Figure S7:** Boxplots with linear mixed models pairwise comparison with estimated marginal means and Benjamini and Hochberg adjustment of leaf and stomatal traits (area, number, and size) per genotype. Abbreviations follow Table 1. $p < 0.05$. **Figure S8:** Correlation of Random Effects with Pearson coefficient of P_{50} versus T_{VW}/D_{MAX} and T_{PM} and relative importance of stem anatomical traits to P_{12}. (A) P_{50} versus T_{VW}/D_{MAX} and (B) P_{50} versus T_{PM}. (C) Relative importance of the stem anatomical variables contributing to P_{12} variation among the genotypes determined using the Lindemann, Merenda, and Gold (LMG) method.